JAMMER CANCELATION BY USING SPACE-TIME ADAPTIVE PROCESSING

A THESIS SUBMITTED TO
THE GRADUATE SCHOOL OF NATURAL AND APPLIED SCIENCES
OF
MIDDLE EAST TECHNICAL UNIVERSITY

BY

HALİL UYSAL

IN PARTIAL FULFILLMENT OF THE REQUIREMENTS
FOR
THE DEGREE OF MASTER OF SCIENCE
IN
ELECTRICAL AND ELECTRONICS ENGINEERING

SEPTEMBER 2011

Approval of the thesis:

JAMMER CANCELATION BY USING SPACE-TIME ADAPTIVE PROCESSING

submitted by **HALİL UYSAL** in partial fulfillment of the requirements for the degree of
**Master of Science in Electrical and Electronics Engineering Department, Middle East
Technical University** by,

Prof. Dr. Canan Özgen
Dean, Graduate School of **Natural and Applied Sciences**   ———————————

Prof. Dr. İsmet Erkmen
Head of Department, **Electrical and Electronics Engineering**   ———————————

Prof. Dr. Mete Severcan
Supervisor, **Electrical and Electronics Eng. Dept., METU**   ———————————

Examining Committee Members:

Prof. Dr. Yalçın Tanık
Electrical and Electronics Engineering Dept., METU   ———————————

Prof. Dr. Mete Severcan
Electrical and Electronics Engineering Dept., METU   ———————————

Prof. Dr. Sencer Koç
Electrical and Electronics Engineering Dept., METU   ———————————

Assoc. Prof. Dr. Çağatay Candan
Electrical and Electronics Engineering Dept., METU   ———————————

Dr. Ülkü Çilek Doyuran
ASELSAN   ———————————

Date: ———————————

I hereby declare that all information in this document has been obtained and presented in accordance with academic rules and ethical conduct. I also declare that, as required by these rules and conduct, I have fully cited and referenced all material and results that are not original to this work.

Name, Last Name: HALİL UYSAL

Signature   :

ABSTRACT

JAMMER CANCELATION BY USING SPACE-TIME ADAPTIVE PROCESSING

Uysal, Halil

M.Sc., Department of Electrical and Electronics Engineering

Supervisor   : Prof. Dr. Mete Severcan

September 2011, 68 pages

Space-Time Adaptive Processing (STAP) has been widely used in spaceborne and airborne radar platforms in order to track ground moving targets. Jammer is an hostile electronic countermeasure that is being used to degrade radar detection and tracking performance. STAP adapts radar's antenna radiating pattern in order to reduce jamming effectiveness. Jamming power that enters the system is decreased with respect to the adapted radiation pattern. In this thesis, a generic STAP radar model is developed and implemented in simulation environment. The implemented radar model demonstrates that, STAP can be used in order to suppress wideband jammer effectiveness together with ground clutter effects.

Keywords: Space-Time Adaptive Processing, Spaceborne and Airborne Platforms, Ground Moving Target, Clutter, Jammer

ÖZ

UZAY - ZAMAN UYARLAMALI İŞLEMCİ KULLANARAK KARIŞTIRICI BASTIRILMASI

Uysal, Halil

Yuksek Lisans, Elektik ve Elektronik Mühendisliği Bölümü

Tez Yöneticisi　: Prof. Dr. Mete Severcan

Uzay-Zaman Uyarlamalı İşleme (STAP) hava veya uzayda konuşlandırılmış radar sistemlerinde, yerde hareket eden hedeflerin takibi için kullanılmakta olan etkin bir yöntemdir. Karıştırıcı, radarın tespit ve takip performansını düşürmek amacıyla düşman güçlerce kullanılan elektronik karşı tedbir yöntemidir. STAP, düşman güçlerce kullanılan bu karşı tedbirin etkinliğini azaltmak için antenin yayılım örüntüsünü uyarlar. Uyarlanmış anten örüntüsüne bağlı olarak sisteme giren karıştırıcı gücü azaltılır. Bu çalışmada STAP özelliğine sahip radar sistemlerinin genel bir modeli geliştirilmiş ve benzetim ortamında modellenmiştir. Gerçekleştirilen bu model aracılığı ile belirtilen radar sistemlerinin çevre yankısı etkileriyle beraber geniş bantlı elektronik karıştırıcı etkinliğinin bastırılması amacıyla da kullanılabileceği gösterilecektir.

Anahtar Kelimeler: Uzay-Zaman Uyarlamalı İşleme, Hava ve Uzay Konuşlu Radar, Yerde Hareket Eden Hedefler, Çevre Yankısı, Elektronik Karıştırıcı

To my mother, to my father who recently has past away and to my family...

ACKNOWLEDGMENTS

I would like to express my sincere gratitude to my supervisor Prof. Dr. Mete Severcan for his invaluable guidance, advice, criticism, encouragement throughout the development of this thesis.

I am thankful to Prof. Dr. Yalçın Tanık, Prof. Dr. Sencer Koç, Assoc. Prof. Dr. Çağatay Candan and Dr. Ülkü Çilek Doyuran for reviewing this manuscript.

I am also grateful to my colleagues from TÜBİTAK-BİLGEM/İLTAREN for their discussions and heartening words.

Finally and most importantly, I wish to express my deepest gratitude to my family. Not just during my graduate studies but during all my life, they have believed in me and helped me to achieve my goals. Their support has always been invaluable.

TABLE OF CONTENTS

LIST OF TABLES

TABLES

LIST OF FIGURES

FIGURES

CHAPTER 1

INTRODUCTION

Airborne or spaceborne radars employ different kinds of algorithms in order to detect and track ground moving targets. However, processing of ground moving targets, using airborne or spaceborne radar is heavily degraded by the interference sources such as ground clutter and hostile electronic counter measures. Therefore, future airborne radars should be able to suppress both clutter and jamming close to or below the noise level.

The ground clutter seen by an airborne or a spaceborne radar exhibits two dimensional spread along Doppler dimension and azimuth dimension. A potential target can be concealed by clutter echo that originates from the same Doppler frequency as well as the echo originated from same azimuth angle. In early 1970s, Space-Time Adaptive Processing (STAP) is proposed as joint domain signal processing in order to suppress interference. Joint space of azimuth-Doppler is formed via collecting transmitted pulses for multiple sensors.

An airborne or a spaceborne radar that employs space-time adaptive processing utilizes N antenna elements to feed the processor. Antenna elements are well calibrated and assumed to be identical. The output of antenna elements are sampled every PRI (Pulse Repetition Interval) during one CPI (Coherent Processing Interval). All samples collected from every antenna element is directed to processor to make a decision on target existence.

Basic illustration for space-time adaptive processing is given in Figure 1.1. Clutter is coupled between the angle-of-arrival (azimuth) and the Doppler frequency, while barrage jamming is localized in the angle-of-arrival and distributed over all Doppler domain.

In this thesis, we study the interference cancelation via space-time adaptive processing. In most radar applications interference sources such as clutter are eliminated via collecting trans-
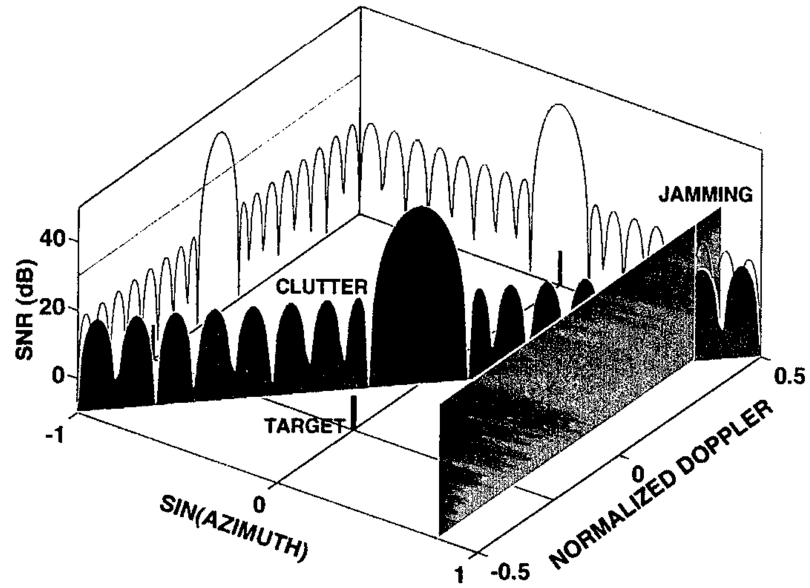
Figure 1.1: Illustration of interference environment for STAP.

mitted pulses from one directive sensor. However, this approach is effective for detecting moving targets, it fails to detect stationary or slowly moving targets due to clutter Doppler spread. Therefore, to see the effectiveness of space-time adaptive processing in interference elimination we modeled a space-time adaptive processing signal simulator and via this simulator we show that space-time adaptive processing can be used effectively to suppress jamming and clutter signals while amplifying the target signal.

1.1   Thesis Outline

In this thesis work, we proposed that space-time adaptive processing can be used for coverage area purposes. Results are tested for different scenario conditions.

In Chapter 2, previous studies on modeling concepts of space-time adaptive processing and basic radar concepts are introduced. Simulation models of jammer, clutter and target are presented.

In Chapter 3, coverage analysis and the need for this tool in radar applications is explained.

In Chapter 4, signal processing tools of space-time adaptive processing are discussed. Effects

of radar system parameters on space-time adaptive processing are investigated.

In Chapter 5, simulation results are discussed. The simulation environment consists of a number of jammer models, clutter model and a target model. Simulation results are compared with conventional pulsed-Doppler radar and a radar that employs space-time adaptive processing via probability of detection.

In Chapter 6, performance of space-time adaptive processing over interference elimination and pros of using space-time adaptive processing for coverage area purposes are discussed, conclusions are done and future works are described

CHAPTER 2

RADAR CONCEPTS AND SPACE - TIME SIGNAL MODELING

The fundamental concepts of radar signal processing is introduced in this chapter along with the moving target indication and temporal processing. Following the discussion on the necessity of STAP, this chapter concludes with developing space-time signal models for target, interference and thermal noise.

2.1   Radar Principles

Radar, an abbreviation standing for *Ra*dio *D*etection *A*nd *R*anging, uses electromagnetic waves for the detection and ranging potential targets. In addition to range typical quantities measured in radars used for search and target tracking are target angles (elevation and azimuth) and target Doppler velocity [1].

In this section, fundamental elements and functions of radars are reviewed [2] - [7].

2.1.1   Fundamental Elements of Radar and Definitions

There are many forms of radar that perform a variety of functions. We will discuss the most elementary structure of pulsed radar and its elements before proceeding with the details. Block diagram of a typical pulsed radar is shown in Figure 2.1. The block diagram is divided into subsystems that will help to the investigation of radar elements. *synchronizer* is the element that controls the timing throughout the system which is also called as *coherent oscillator*. Generated signals in power supply is sent to *modulator* and *Rf amplifier* path according to

4

the signals sent from synchronizer. Pulsed radars employ one *antenna* for receive and transmit operations and switching operation of transmitting and receiving modes is controlled by *duplexer*. After, radar transmits a pulse it turns into listening mode where duplexer is in receive mode. Received signals are preamplified and downconverted to intermediate frequency (IF). The signal processor provides the detection, tracking functions as well as processing need for display purposes.
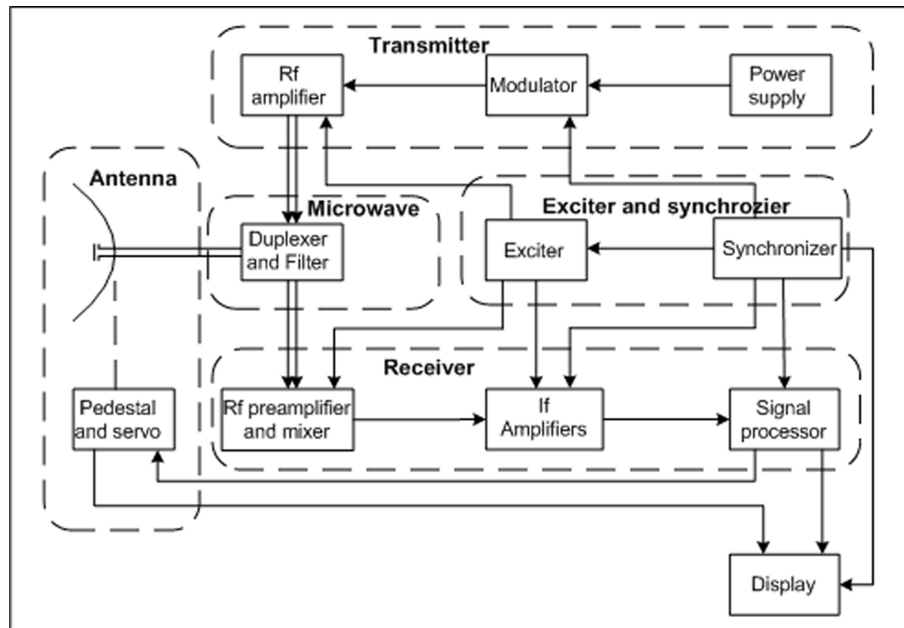
Figure 2.1: Block diagram of a typical pulsed radar.

2.1.1.1 Range to a Target

Target's range, R, is computed by measuring the time delay, Δt, between transmitted and received pulsed signal. The situation is demonstrated in Figure 2.2. Target range is related to the time delay through

$$R = \frac{c\Delta t}{2},$$ (2.1)

where c is the velocity of light.
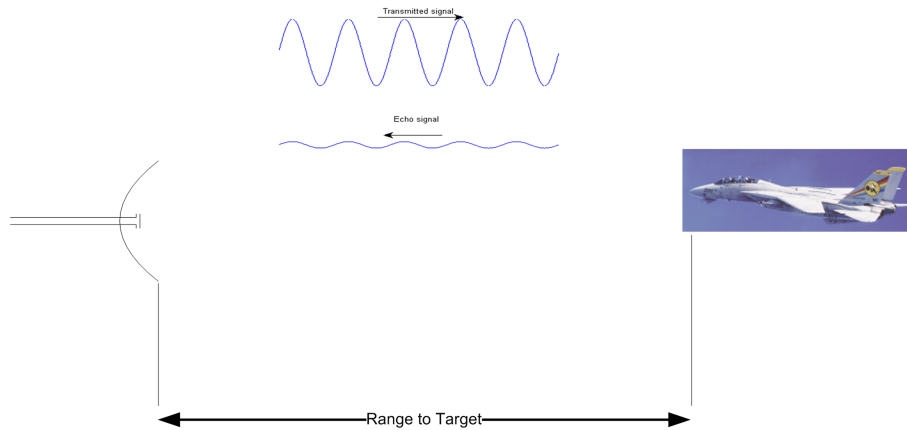
Figure 2.2: Simplified range diagram.

2.1.1.2 Maximum Unambiguous Range

Typically, a pulsed radar transmits a sequence of pulses, which is called a *pulse train*, as illustrated in Figure 2.3
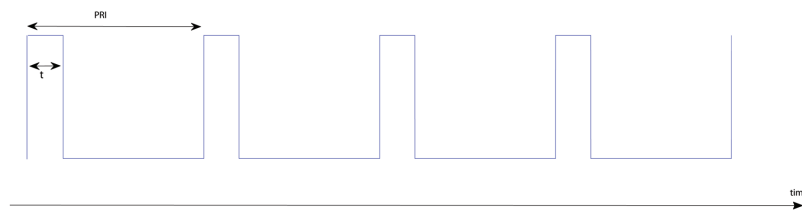
Figure 2.3: Demonstration of a pulse train.

The duration between transmitted pulses is often called as Pulse Repetition Interval (PRI). This interval limits the *maximum unambiguous range* for a pulsed radar. This is the range for which a reflection from the previous transmitted pulse is received at the transmission instant of the next pulse. Maximum unambiguous range, R_u, is given by

$$R_u = \frac{cT}{2},\qquad(2.2)$$

where T is the pulse repetition interval. Echoes from objects at ranges greater than the unambiguous range will appear at much closer ranges. This is known as *Range Ambiguity*.
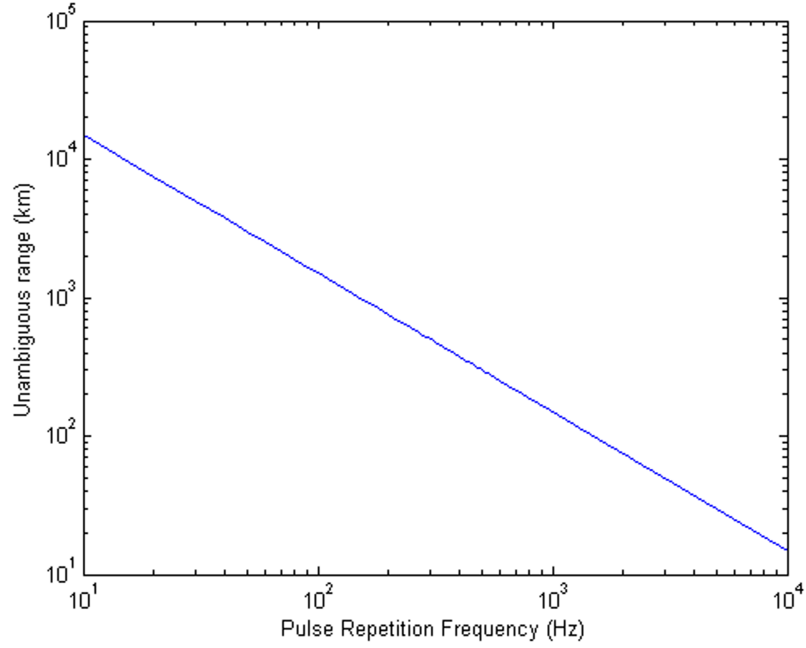
Figure 2.4: Unambiguous range with respect to PRF.

2.1.1.3 Target Velocity

Radars use Doppler frequency to extract target *radial* velocity. Doppler phenomenon describes the shift in the center frequency of the radiated wave due to the target motion with respect to the source. For the sake of simplicity, assume that the radiating source is moving with radial velocity, v_{rad}, and reflecting object is stationary. The frequency, f_1, received by the target for the radiating frequency, f_0, is predicted by the theory of relativity and it is given as,

$$f_1 = f_0 \frac{c + v_{rad}}{\sqrt{c^2 - v_{rad}^2}}, \tag{2.3}$$

where f_0 is the transmitting frequency. Defining Doppler shift as $f_d = f_1 - f_0$ and using the fact that the radial velocity is very small compared to the speed of light, eq. (2.3) can be reduced to

7

$$f_d = \frac{f_0 v_{rad}}{c} = \frac{v}{\lambda}, \tag{2.4}$$

where λ is wavelength. The reflection from the fixed object may be viewed as a reradiation at frequency f_1. Therefore, the total Doppler shift observed is twice one the given in eq.(2.4)

$$f_d = \frac{2 f_0 v_{rad}}{c} = \frac{2v}{\lambda}. \tag{2.5}$$

2.1.2 Radar Range Equation

The *radar range equation* is a deterministic model that relates the received echo power, P_r, to the transmitted power, P_t, in terms of system parameters.

The first step of deriving the radar range equation is finding the power density, S_t, at a range R due to an isotropic transmitter antenna, which is

$$S_t = \frac{P_t}{4\pi R^2}. \tag{2.6}$$

But in practice, antennas radiate directionally. The maximum gain of a directive antenna, G_t, is defined as the ratio of the radiated power density at the boresight to the isotropic power density. Therefore, eq.(2.6) becomes

$$S_t = \frac{P_t G_t}{4\pi R^2}. \tag{2.7}$$

Eq. (2.7) gives the power density incident upon the target. Of course, S_t is now a function of the direction of the target. For the sake of simplicity, let us assume that the target is aligned with the maximum gain of antenna, G. Now, assume that the power density given by eq.(2.7) is incident upon a *point target* at a range R. This incident energy will be reflected back according to the *radar cross section* (RCS), σ, of the target and the target reradiates the incident energy isotropically. Reradiated power from the point target is given by

$$P_c = S_t \sigma = \frac{P_t G \sigma}{4\pi R^2}. \tag{2.8}$$

8

Since RCS is defined under the assumption that the target reradiates the collected power isotropically, the power density at the radar receiver is found by

$$S_r = \frac{P_c}{4\pi R^2} = \frac{P_t G \sigma}{(4\pi)^2 R^4}.$$

(2.9)

The total power collected by the receiving antenna is

$$P_r = S_r A_r = \frac{P_t G A_r \sigma}{(4\pi)^2 R^4},$$

(2.10)

where A_r is the receiving cross section of the antenna. The receiving cross section of an antenna is related to its gain, G, and operating wavelength, λ, as

$$A_r = \frac{G\lambda^2}{4\pi}$$

(2.11)

Using eq.(2.11) in eq.(2.10) we find the radar range equation as

$$P_r = \frac{P_t G^2 \lambda^2 \sigma}{(4\pi)^3 R^4}.$$

(2.12)

2.2 Moving Target Indication

In addition to the reflection from the target, emitted radar waves are also reflected from the structures within the resolution cell such as terrain, forest, vegetation, sea etc. These unwanted reflections are called as *clutter*. There are many radar applications in which clutter is stationary relative to the radar. From 2.1.1.3, we know that Doppler frequency of a moving object is used to find its velocity. If clutter is stationary relative to the radar then, the clutter's Doppler spectrum will be around zero frequency. Therefore, most of the clutter echo will be removed if the near-zero Doppler spectrum is filtered out. This filtering process is called as *moving target indication*, (MTI).

This section describes moving target indication techniques such as *pulse cancelers* and *temporal processing*. Though, pulse cancelers filters near-zero Doppler spectrum, temporal processing

9

utilizes all Doppler spectrum with successive filters centered at different frequencies. Visualization of temporal processing as Doppler filter bank is given in Figure 2.5 [8, 9, 10].
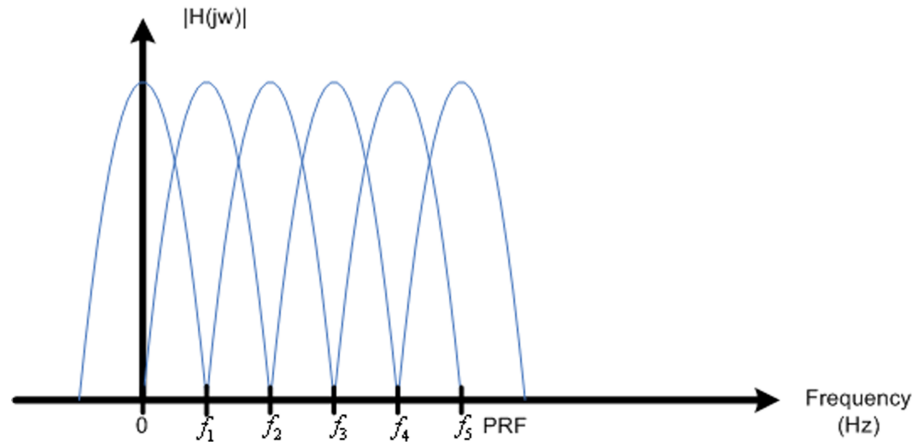
Figure 2.5: Doppler filter banks.

2.2.1 Pulse Cancelers

The major design issue of MTI filter is the choice of the particular degree of MTI filter to be used for clutter suppression. The most common MTI filters are based on very simple design approaches. Now, imagine that a landbased radar is illuminating a moving target surrounded by perfectly stationary clutter. The clutter component of the echo will be identical for every pulse to be transmitted, while the phase of the moving target component would vary with the changes in range. Subtracting successive pulses would cancel the clutter components while the target signal would not be canceled due to the phase change in received echo.

Degree of the pulse canceler is determined from the number of pulses used in the filtering process.

2.2.1.1 Two Pulse Canceler

Two pulse canceler uses two successive pulses to suppress clutter. Two pulse canceler is also called as *single delay line canceler* since it contains only one delay element. The graphical demonstration of a two pulse canceler is shown in Figure 2.6, where the delay time T must be equal to the pulse repetition interval of the radar.

10
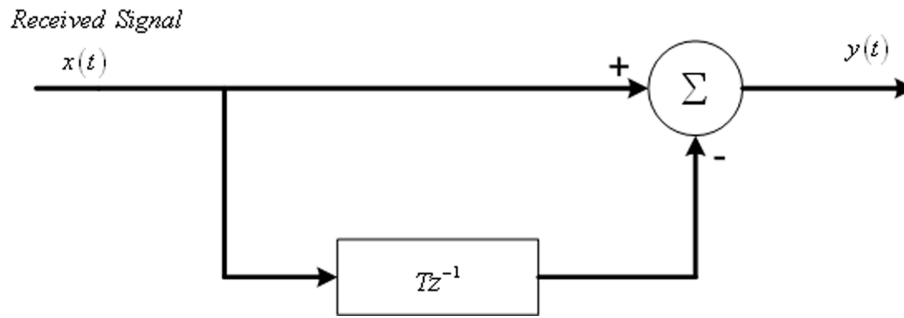
Figure 2.6: Two pulse canceler

The time domain output of the two pulse canceler can be written as

$$y(t) = x(t) - x(t - T).$$ (2.13)

The frequency response of the two pulse canceler can easily be shown as Fourier transform of eq.(2.13):

$$|H(\omega)| = 2 \left| \sin \frac{\omega T}{2} \right|.$$ (2.14)

2.2.1.2 Three Pulse Canceler

Three pulse canceler is effectively two cascaded two pulse cancelers as it is shown in Figure 2.7
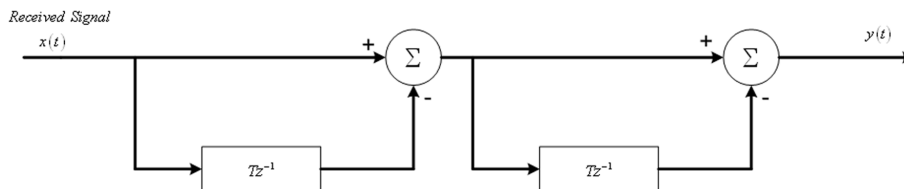
Figure 2.7: Three pulse canceler.

The time domain output of the three pulse canceler can be written as

11

$$y(t) = x(t) - 2x(t - T) + x(t - 2T).$$ (2.15)

The frequency response of the three pulse canceler can easily be shown as Fourier transform of eq.(2.15):

$$|H(\omega)| = 4\sin^2\left(\frac{\omega T}{2}\right).$$ (2.16)

Figure 2.8 illustrates the frequency responses of two and three pulse cancelers.
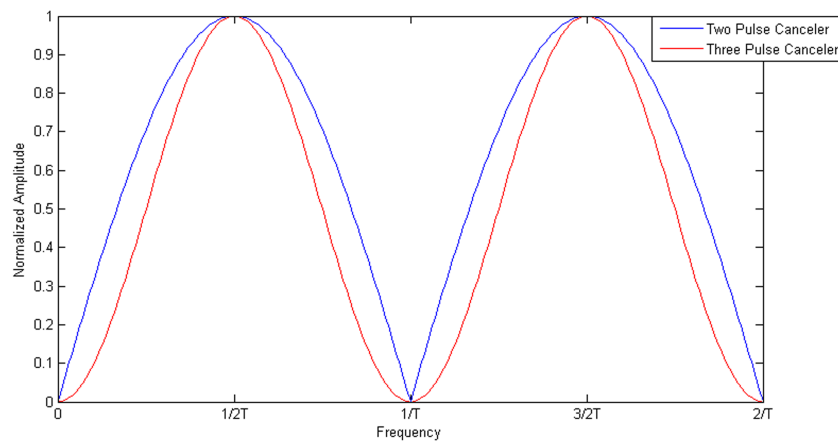
Figure 2.8: Frequency response of two and three pulse cancelers.

2.2.2 Temporal Processing

Radar data matrix is a tool that illustrates the received samples in a structure. Figure 2.9 illustrates the radar data matrix. The columns are the samples of the received signal at each range bin while the rows are the samples at a given range for each transmitted pulse. We know that moving target's successive echo phase will vary and we also know that the derivative of phase with respect to time is the definition of instantaneous frequency. Starting with the definition of frequency and using the successive samples taken from one range bin we can determine the Doppler frequency of the target [11].

As mentioned before, there is range ambiguity because of PRI. Same kind of ambiguity exists
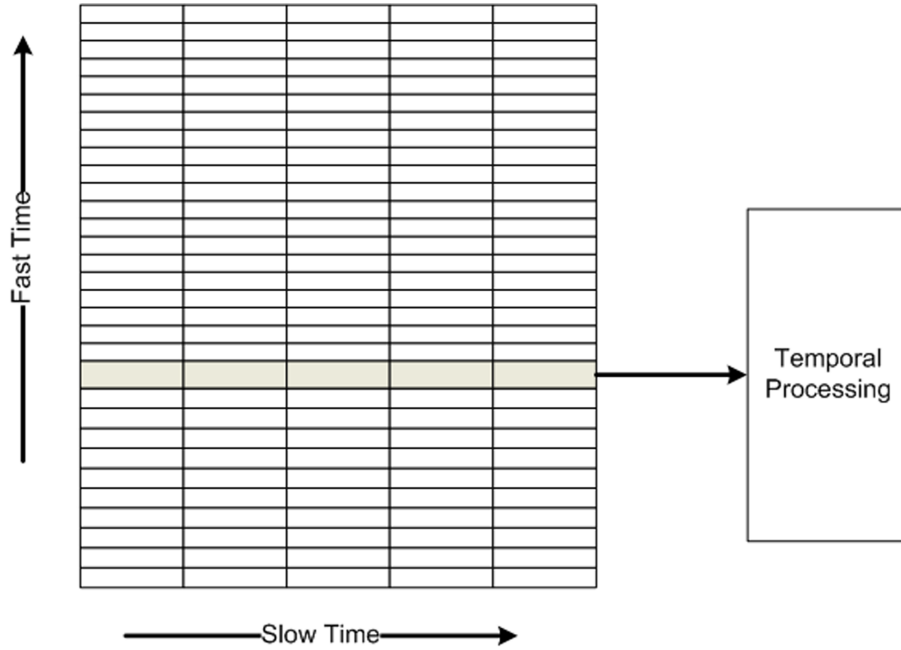
Figure 2.9: Fast time slow time data matrix.

in temporal processing. As we know from the sampling of continuous signals, frequency spectrum of the sampled signal repeats itself with sampling frequency. Since we sampled the continuous range signals with PRF in slow time, the spectrum is periodic with PRF. If there is a target with Doppler frequency above PRF, there will be ambiguity. As it is explained in 2.1.1.3 there is a relation between Doppler frequency and radial velocity of the target. The maximum resolvable Doppler frequency is the sampling frequency, namely PRF. By using the relation between Doppler frequency and velocity, the maximum unambiguous velocity of a system, v_{max}, is given by

$$v_{\max} = \frac{PRF\lambda}{2}. \tag{2.17}$$

2.3 The Need for Space - Time Adaptive Processing and Tools for Spectral Estimation.

The fundamental reasoning for STAP relies on the two dimensional nature of ground clutter for airborne or spaceborne radars. Ground clutter for airborne or spaceborne radars is dis-

13

tributed along azimuth and Doppler dimensions. Figure 2.10 illustrates [10] the distribution of ground clutter for side-looking radar employing *uniform linear array* (ULA). In a uniform linear array, sensors used in the antenna array of the radar are distributed on a line with equal displacements.
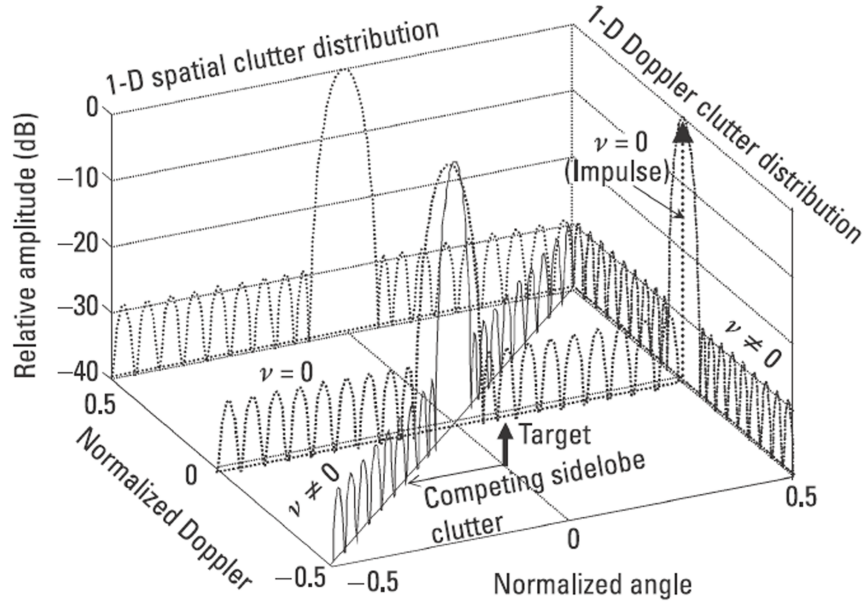
Figure 2.10: Ground clutter for side-looking uniform linear array (ULA)

2.3.1 Spectral Estimation

In this section, tools for spectral analysis will be explained. The spectral estimation tools considered in this section are based on the covariance matrix of the received signal $\mathbf{R} = E\left\{\mathbf{x}\mathbf{x}^H\right\}$ where, $\mathbf{x}$ includes all signal components, target signal, interference signal and noise. Power spectral estimators might be divided into two subsections, *signal match* and *super resolution* type.

2.3.1.1 Signal Match

Signal match spectral estimator uses matched filter in order to calculate the estimation [12]. Signal match estimator is given in eq. (2.18). This estimator uses a search algorithm along

14

Doppler dimension (f_D) and azimuth dimension (φ).

The estimation, P_{SM}, is obtained by

$$P_{SM}(\varphi, f_D) = \frac{\mathbf{s}^H(\varphi, f_D)\,\mathbf{R}\mathbf{s}(\varphi, f_D)}{\mathbf{s}^H(\varphi, f_D)\,\mathbf{s}(\varphi, f_D)}, \tag{2.18}$$

where $\mathbf{s}$ conforms the search algorithm in two dimensions and $\mathbf{R}$ is the covariance matrix of the received signal $\mathbf{x}$.

2.3.1.2 Minimum Variance Estimation

Minimum variance estimation is the optimum processor spectral estimation. Minimum variance estimation does not involve spurious sidelobes that we observe in signal match estimator. Minimum variance estimation is based on the statistics of the data received by the array, $\mathbf{x}(t)$. The data received by the array is composed of interference signal, $\mathbf{i}(t)$, noise signal, $\mathbf{n}(t)$ and the target signal, $\mathbf{s}(t)$. The goal is to optimize the beamformer response, so that the output contains minimum contributions due to noise and interference other than the desired signal direction. This approach is also called as *Minimum Variance Distortionless Response* (MVDR). The derivation of this method is given through eq. (2.19) - eq. (2.25). Let

$$\begin{aligned} \mathbf{x}(t) &= \mathbf{s}(t) + \mathbf{i}(t) + \mathbf{n}(t) \\ \mathbf{e}(t) &= \mathbf{i}(t) + \mathbf{n}(t) \end{aligned} \tag{2.19}$$

where $\mathbf{x}(t)$ is the received total signal and $\mathbf{e}(t)$ is the total interference plus noise signal. Interference is a term used for unwanted echoes from clutter and received signal from jammers.

The cost function that defines minimum variance estimator is given by

$$SINR = \max_{\mathbf{w}} \frac{\mathbf{w}^H \mathbf{s}(\varphi, f_D)\,\mathbf{R_s}\mathbf{s}^H(\varphi, f_D)\,\mathbf{w}}{\mathbf{w}^H \mathbf{R_e} \mathbf{w}}, \tag{2.20}$$

where $\mathbf{w}$, $\mathbf{R_s}$ and $\mathbf{R_e}$ are weight vector for filter, covariance matrices of the desired signal and covariance matrix of the interference plus noise, respectively. The first assumption of this derivation is $\mathbf{w}^H \mathbf{R_e} \mathbf{w} = const$ and we know what we have transmitted, the covariance matrix

of the desired signal is nothing but an identity matrix multiplied with its power, $\mathbf{R_s} = \sigma_s \mathbf{I}$. Therefore, eq. (2.20) becomes

$$SINR = \max_{\mathbf{w}} \frac{\mathbf{w}^H \mathbf{s}(\varphi, f_D) \mathbf{s}^H(\varphi, f_D) \mathbf{w}}{\mathbf{w}^H \mathbf{R_e} \mathbf{w}}. \tag{2.21}$$

To maximize eq. (2.21) we need to minimize its denominator.

$$\min_{\mathbf{w}} \mathbf{w}^H \mathbf{R_e} \mathbf{w} \quad such \quad that \quad \mathbf{w}^H \mathbf{s}(\varphi, f_D) = 1. \tag{2.22}$$

To minimize eq. (2.22) *Lagrange Multiplier Method* can be used.

$$E = \mathbf{w}^H \mathbf{R_e} \mathbf{w} + \lambda \left(1 - \mathbf{w}^H \mathbf{s}(\varphi, f_D) \right)$$
$$\frac{\partial E}{\partial \mathbf{w}^H} = \mathbf{R_e} \mathbf{w} - \lambda \mathbf{s}(\varphi, f_D) = 0 \tag{2.23}$$

which yields

$$\mathbf{w} = \lambda \mathbf{R_e}^{-1} \mathbf{s}(\varphi, f_D). \tag{2.24}$$

By using the condition given in eq. (2.22) in eq. (2.24), we find the minimum variance estimator as [12]

$$\lambda = \frac{1}{\mathbf{s}^H(\varphi, f_D) \mathbf{R_e}^{-1} \mathbf{s}(\varphi, f_D)}. \tag{2.25}$$

Minimum variance estimator algorithm also employs a search algorithm along Doppler dimension and azimuth dimension as

$$P_{MSE}(\varphi, f_D) = \frac{1}{\mathbf{s}^H(\varphi, f_D) \mathbf{R_e}^{-1} \mathbf{s}(\varphi, f_D)}. \tag{2.26}$$

2.3.1.3 MUSIC

MUSIC stands for *Mu*ltiple *S i*gnal *C*lassification and the principle of MUSIC is orthogonal projection over interference eigenspace. MUSIC is one of the most powerful method for

super resolution spectral estimation techniques. It can be applied to any array geometry but it requires a search algorithm as it is explained in 2.3.1.2 [12]. MUSIC has a similar form to minimum variance estimation

$$P(\varphi, f_D) = \frac{1}{\mathbf{s}^H(\varphi, f_D)\mathbf{G}\mathbf{G}^H\mathbf{s}(\varphi, f_D)}, \quad (2.27)$$

where $\mathbf{G}$ is defined as the eigenvectors that spans the noise-interference space of the total covariance matrix, $\mathbf{R}$. In this algorithm, main drawback is separating the eigenvalues of signal space and noise-interference space.

2.4 Space - Time Signal Modeling

This section describes the space-time signal model that will be used in the rest of this work. Using the geometry of an array located on a spaceborne or an airborne radar, space-time signal model for a motionless point scatterer is derived. This signal model is then extended to include target and interference responses as well.

2.4.1 Array Geometry

Geometry of airborne or spaceborne radar which employs a linear array is demonstrated in Figure 2.11. Throughout this thesis, it is assumed that radar platform moves in the x-direction, x-direction is defined as zero azimuth reference. Also, flat earth model is used for propagation purposes therefore, depression angle, θ is equal to elevation angle. R_s is the slant range between radar and reflecting point, R_g is the ground range, ϕ denotes the azimuth angle between moving direction and the reflecting point and v_p is the platform velocity [13, 14, 15].

Another assumption about received signal is that it is narrowband, which means that the received signal travels through the array without any time difference, which means that the first sensor and the last sensor in the array senses the received signal at the same time only, spatial phase difference in between the received signals of each sensor is given by

$$\Delta\varphi = j\frac{2\pi}{\lambda}((x_i\cos\varphi + y_i\sin\varphi)\cos\theta - z_i\sin\theta) \quad i = 1...N, \quad (2.28)$$
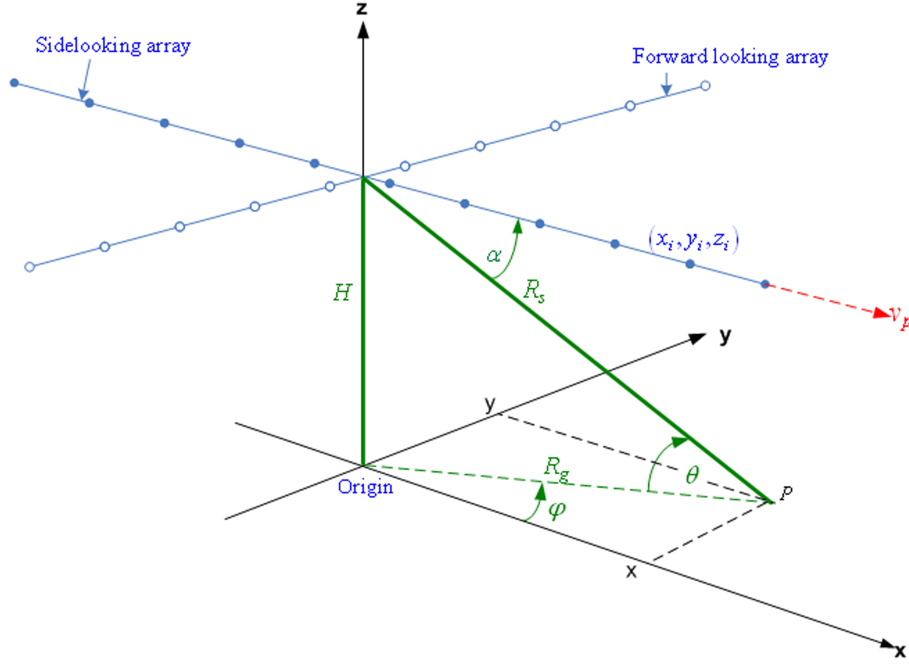
Figure 2.11: Geometry of a linear array located on an airborne radar.

where x_i, y_i, z_i are the coordinates of the ith sensor relative to the origin and N is the number of the array elements.

2.4.2 Received Signal From Stationary Scatterer

For the geometry shown in Figure 2.11 the signal received for a sensor placed at x_i, y_i, z_i due to a stationary scatterer is

$$s_r = A(\varphi) \exp\left[j\tfrac{2\pi}{\lambda} \left(\left(\left(x_i + 2v_p mT\right) \cos\varphi + y_i \sin\varphi \right) \cos\theta - z_i \sin\theta \right) \right] ,$$
$$m = 1...M \quad i = 1...N$$

(2.29)

where m is the operating pulse in CPI and i is the sensor that received the signal.

2.4.3 Received Signal From Moving Scatterer

For a moving scatterer with radial velocity, v_{rad}, with respect to the platform that carries the radar, then by using v_{rad} in eq. (2.29), received signal for moving scatterer becomes

$$s_r = A\left(\varphi\right)\exp\left[j\frac{2\pi}{\lambda}\left(2v_{rad}mT + (x_i\cos\varphi_t + y_i\sin\varphi_t)\cos\theta - z_i\sin\theta\right)\right]$$

$$m = 1...M \quad i = 1...N \tag{2.30}$$

where v_{rad} is the radial velocity which includes the target radar geometry and also the scatterer's velocity and cruise direction, φ_t is the scatterer's azimuth with respect to the radar.

2.4.4 Interference Signal Modeling

This section contains the signal models for the ground clutter and jamming.

2.4.4.1 Ground Clutter

The assumptions given in [13] for clutter echoes are also followed in this work, and they are given below for the sake of completeness:

- Echoes of different scatterers are independent and identically distributed. And due to central limit theorem [16] they are asymptotically Gaussian.

- Temporal clutter fluctuations are slow compared with the observation time.

- The clutter returns are due to the regions in line-of-sight of the radar, hence diffraction effects are omitted.

The total clutter echo for a single range cell, c_{im}, is found by integrating the received signal given in eq. (2.29) over all azimuth angles

$$
\begin{aligned}
c_{im} &= \int_{\varphi=0}^{\varphi=2\pi} s_r\left(\varphi\right)d\varphi \\
&= \int_{\varphi=0}^{\varphi=2\pi} A\exp\left[j\frac{2\pi}{\lambda}\left(\left(\left(x_i + 2v_pmT\right)\cos\varphi + y_i\sin\varphi\right)\cos\theta - z_i\sin\theta\right)\right]d\varphi
\end{aligned}
\tag{2.31}
$$

$$m = 1...M \quad i = 1...N$$

where A is a circular complex Gaussian distributed random variable [17]. It can be seen that eq. (2.31) can be divided into two parts where one part forms temporal phase term and other part forms spatial phase term as

$$\Phi_m\left(v_p, \varphi\right) = \exp\left[j\tfrac{2\pi}{\lambda} 2v_p mT \cos\varphi \cos\theta\right]$$

$$\Psi_i\left(\varphi\right) = \exp\left[j\tfrac{2\pi}{\lambda}\left(x_i \cos\varphi + y_i \sin\varphi\right)\cos\theta - z_i \sin\theta\right] \qquad (2.32)$$

Till now, we have included neither receive directivity nor transmit directivity in the equations we derived. We know that directivity patterns are included as signal gain multipliers. Therefore, received signal from stationary clutter patch is given as

$$c_{im} = \int_{\varphi=0}^{\varphi=2\pi} A D\left(\varphi\right) G\left(\varphi, m\right) \Phi\left(v_p, \varphi\right) \Psi\left(\varphi\right) d\varphi, \qquad (2.33)$$

where $G\left(.\right)$ stands for the transmit directivity pattern and $D\left(\varphi\right)$ is used for receive directivity pattern. The receive directivity pattern $D\left(.\right)$ can be modeled as

$$D\left(\varphi\right) = 0.5\left(1 + \cos\left(2\left(\varphi - \varphi_0\right)\right)\right), \qquad (2.34)$$

$$D\left(\theta\right) = 0.5\left(1 + \cos\left(2\left(\theta - \theta_0\right)\right)\right), \qquad (2.35)$$

while the transmit directivity pattern can be written as

$$G\left(\varphi, \theta\right) = \mathbf{b}(\varphi_L, \theta)^H \mathbf{b}\left(\varphi, \theta\right) \qquad (2.36)$$

where φ_{L} is the look direction. Throughout this thesis it is assumed that $\varphi_{\mathrm{L}} = 0°$ for forward looking array and $\varphi_{\mathrm{L}} = 90°$ for sidelooking array configuration. $\mathbf{b}$ is a beamformer with elements, b_i,

$$b_i\left(\varphi, \theta\right) = \exp\left[j\tfrac{2\pi}{\lambda}\left(\left(x_i \cos\varphi + y_i \sin\varphi\right)\cos\theta - z_i \sin\theta\right)\right] \quad i = 1...N \qquad (2.37)$$

where N is the number of transmit elements in the array.

Up to now, we did not take into account the internal clutter motion. Since, any moving scatterer will vary the temporal phase, then the temporal phase term defined in eq (2.32) will include radial velocity of clutter motion with respect to the platform that carries the radar. So, temporal phase term for moving clutter becomes

$$\Phi_m\left(\varphi, v_p, v_c\right) = \exp\left[j\frac{2\pi}{\lambda}\left(v_p\cos\varphi\cos\theta + v_c\right)2mT\right]. \tag{2.38}$$

Hence, if we are dealing with moving clutter we may use eq. (2.38) in eq. (2.33).

2.4.4.2 Jamming

In this thesis, barrage noise jamming is assumed. The received jamming signal by the ith sensor of the array at time m due to J jammers is

$$c_{im}^{(j)} = \sum_{j=1}^{J} A_j(m)\exp\left[j\frac{2\pi}{\lambda}\left(\left(x_i\cos\varphi_j + y_i\sin\varphi_j\right)\cos\theta_j - z_i\sin\theta_j\right)\right], \tag{2.39}$$

where A_j's are jammer amplitudes and φ_j and θ_j's are the angles that determine angular the positions of the jammers with respect to the radar. Jammer amplitudes are also defined as circular complex Gaussian distributed random variable.

2.4.5 Noise

Besides the interference sources, the inevitable internal noise is modeled as

$$\mathbf{n} = \left[\begin{array}{cccc} n_1 & n_2 & ... & n_{MN} \end{array}\right], \tag{2.40}$$

where n_i's are independent white Gaussian random variable [14].

2.4.6 Properties of Airborne Interference

The properties of the airborne/spaceborne interference signals such as space-Doppler characteristics, space-time covariance matrix and associated azimuth-Doppler spread are given in this section.

2.4.6.1 Doppler-Azimuth Clutter Trajectories

From eq. (2.29) we can deduce that clutter Doppler frequency is colored since for any pair of azimuth elevation angles individual clutter patch has its own Doppler frequency. Clutter Doppler frequency due to stationary scatterer on the ground is proportional to the radial velocity between the platform and the scatterer (see 2.1.1.3 and Figure 2.11).

$$
\begin{aligned}
f_D &= \tfrac{2v_p}{\lambda} \cos \alpha \\
f_D &= \tfrac{2v_p}{\lambda} \cos \varphi \cos \theta
\end{aligned}
\qquad (2.41)
$$

According to eq. (2.41), the signal Doppler badwidth

$$
Clutter\,Doppler\,S\,pread = \left[\; -\tfrac{2v_p}{\lambda} \cos \theta \quad \tfrac{2v_p}{\lambda} \cos \theta \; \right]. \qquad (2.42)
$$

Hence the maximum spread of the clutter in Doppler domain is, $\tfrac{2v_p}{\lambda} \cos \theta$. Notice that clutter spread is larger at long ranges (small θ).

Now, for the sake of simplicity let us define relative Doppler frequency as

$$
f_r = \frac{f_D \lambda}{2v_p} = \cos \varphi \cos \theta \qquad (2.43)
$$

From array geometry given in Figure 2.11 we obtain the following relations

$$
\cos \varphi = \tfrac{x_p}{R_s} \quad \cos \theta = \tfrac{R_g}{R_s} \qquad (2.44)
$$

where, R_s and R_g are defined as $R_g = \sqrt{x_p^2 + y_p^2}$, $R_s = \sqrt{R_g^2 + H^2}$ respectively. So, relative Doppler frequency given in eq. (2.43) becomes

$$
f_r = \frac{x_p}{\sqrt{H^2 + x_p^2 + y_p^2}} \qquad (2.45)
$$

After a few algebraic manipulations eq. (2.45) becomes a set of hyperbolas which define the iso-Doppler (isodop) curves.

$$\frac{x_p^2}{H^2 f_r^2/(1-f_r^2)} - \frac{y_p^2}{H^2} = 1 \quad f_r = \begin{bmatrix} -1 & 1 \end{bmatrix} \tag{2.46}$$

Figure 2.12 shows such a set of hyperbolas.
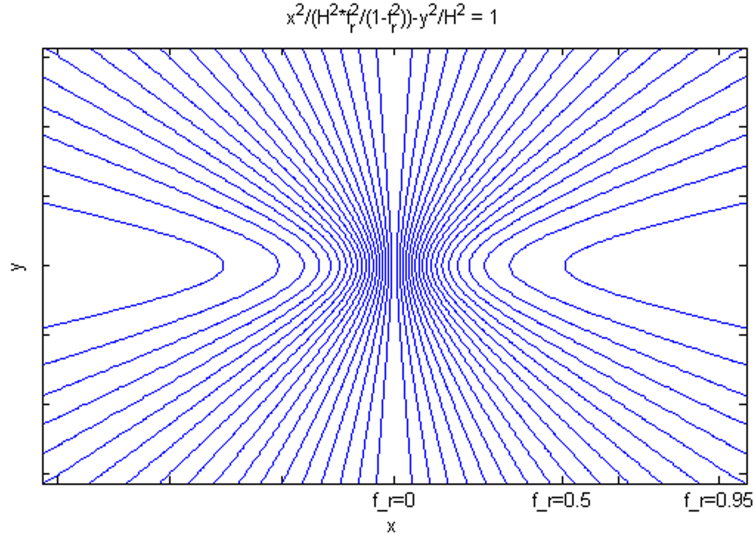
Figure 2.12: Iso-Doppler (isodop) curves.

Until now, we derive the trajectories for range and azimuth axes, isodops. As next step we will derive the trajectories of clutter spectra in Doppler-azimuth plane. The array that is used for transmit and receive processes is assumed to be linear and it is misaligned from the velocity vector by ψ angle. The look direction, β, of the array is depicted in Figure 2.13.

Since we are focusing on Doppler-azimuth plane there is no range increment. Therefore, the depression angle θ is constant. Now, using the relation given in eq. (2.45) we obtain

$$f_r^2 - 2f_r \cos\beta \cos\psi + \cos^2\beta = \sin\psi \cos^2\theta. \tag{2.47}$$

The relation between Doppler and azimuth is depicted in Figure 2.14 for different θ angles and for different crab angles, ψ [10, 13, 14, 18].

The depression angle is varied by changing slant range (R) or height (H). Therefore, it has been plotted for different θ angles by changing R/H.

23
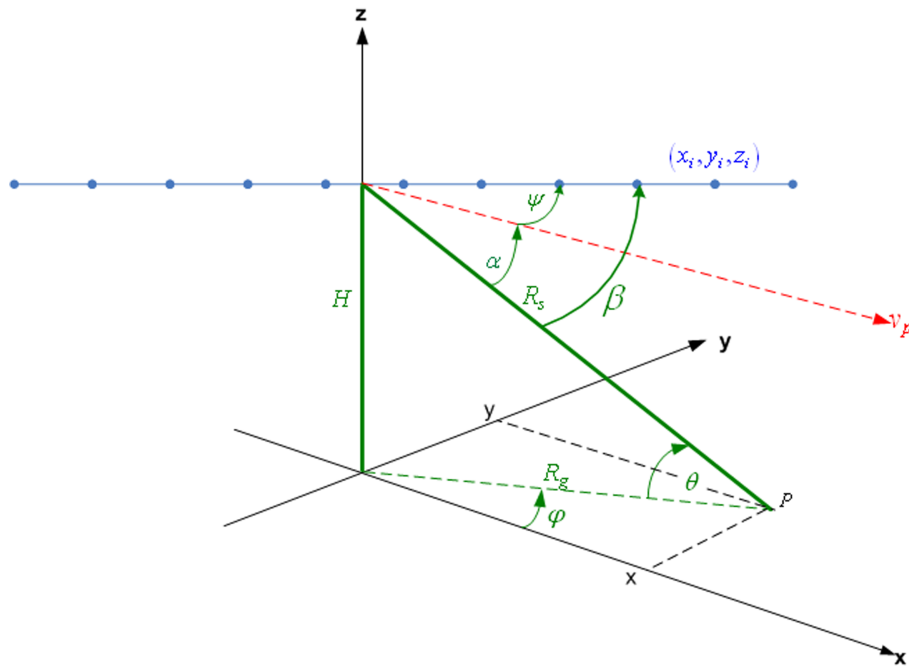
Figure 2.13: Geometry of a linear airborne array with crab angle.
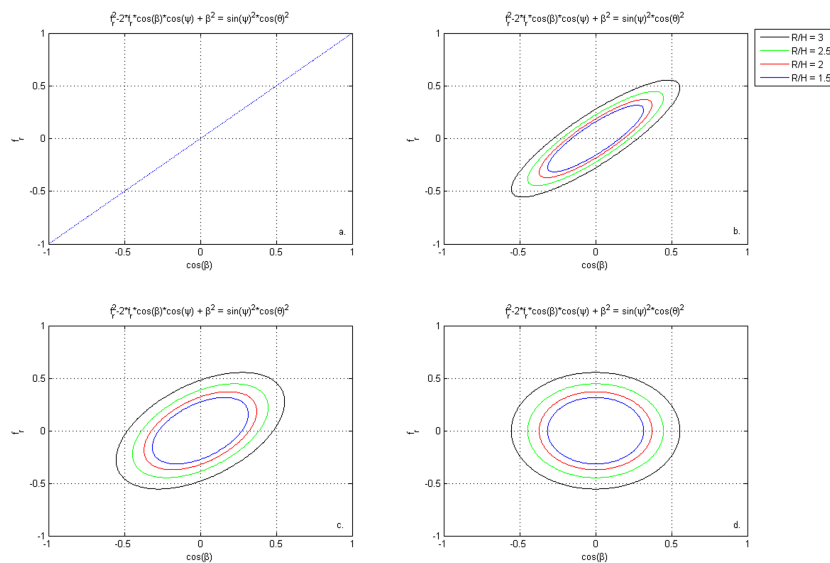
Figure 2.14: Clutter trajectories: a. $\psi = 0°$ b. $\psi = 30°$ c. $\psi = 60°$ d. $\psi = 90°$

2.4.6.2 Clutter Covariance Matrix

The elements of the space-time clutter covariance matrix are composed of the expectation of the clutter echoes given in eq. (2.33) [17, 19]

$$q_{ln}^c = E\left\{c_{im}c_{kp}^*\right\} \tag{2.48}$$

where * is conjugation and subindexes l, n are defined as

$$l = (m-1)N + i \quad m = 1...M; \quad i = 1...N$$
$$n = (p-1)N + k \quad p = 1...M; \quad k = 1...N \tag{2.49}$$

In eq. (2.33), the only statistical contribution comes from the amplitude of the received echo. From the assumptions we have made in modeling the clutter signal, we readily can conclude that echoes from different clutter scatterers are mutually independent from eachother:

$$E\left\{A(\varphi)A^*(\phi)\right\} = 0 \quad \varphi \neq \phi \ . \tag{2.50}$$

Eq. (2.50) means that the cross-terms in azimuth are vanished. Therefore, by using eq. (2.33) in expectation, every clutter covariance element in clutter covariance matrix becomes

$$q_{ln}^{(c)} = P_c\rho(mp) \int_{\varphi=0}^{2\pi} \rho(\tau_{ik})\, D^2(\varphi)\, G(\varphi,m)G^*(\varphi,m)\, \Phi_m\left(\varphi,v_p\right)\Phi_p^*\left(\varphi,v_p\right) \Psi_i(\varphi)\, \Psi_k^*(\varphi)\, d\varphi, \tag{2.51}$$

where indices l, n, m, p, i, k are defined in eq. (2.49).

The functions $\rho(mp)$ and $\rho(\tau_{ik})$ presented in eq. (2.51) are spatial and temporal decorrelation functions, respectively. Spatial decorrelation function is determined with respect to the signal bandwidth and the time that is required for an incoming wave to travel between sensors i and k. The signal bandwidth is represented with δ and the travel time is defined as

$$\tau_{ik} = \frac{1}{c}\left[((x_i - x_k)\cos\varphi + (y_i - y_k)\sin\varphi)\cos\theta - (z_i - z_k)\sin\theta\right] \tag{2.52}$$

where, x, y, z are the cartesian coordinates of the ith and k^{th} sensors. Therefore, spatial decorrelation is defined as

$$\rho\left(\tau_{ik}\right) = \begin{cases} 1 - \frac{|\tau_{ik}|}{\delta} & : t = [-\delta, \delta] \\ 0 & : \text{otherwise} \end{cases}. \tag{2.53}$$

Temporal decorrelation is affected by the internal clutter motion. It is assumed that the clutter fluctuations have Gaussian correlation given as:

$$p_c\left(t\right) \triangleq \exp\left(-\frac{\sigma^2}{2}\tau^2\right). \tag{2.54}$$

The power spectrum of the Gaussian correlation function is again a Gaussian function,

$$P_c\left(\omega\right) = \sqrt{\frac{2\pi}{\sigma^2}} \exp\left(-\frac{\omega^2}{2\sigma^2}\right), \tag{2.55}$$

where bandwidth of Gaussian shaped correlation function is defined as, $B = 2\sigma$. Since, temporal decorrelation occurs in between successive pulses, the elapsed time τ is defined as $\tau = (m - p) \times PRI$. Temporal decorrelation becomes

$$\rho\left(mp\right) = \exp\left(-\frac{B_c^2\left(m - p\right)^2}{8}\right). \tag{2.56}$$

where B_c is the normalized clutter fluctiation bandwidth given as:

$$B_c = B/PRF = B \times PRI. \tag{2.57}$$

Figure 2.15 shows clutter covariance matrix for a uniform linear array employing omni directional sensors with $M = 7$ and $N = 14$.
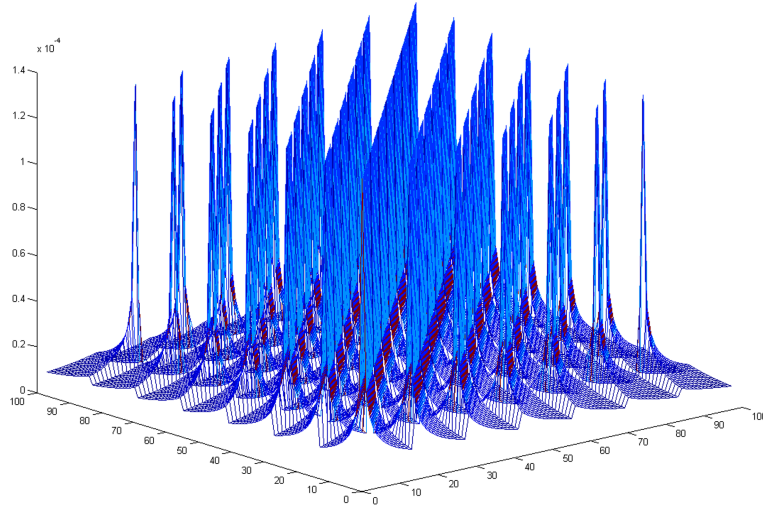
Figure 2.15: Clutter covariance matrix for M=7 and N=14.

2.4.6.3 Jammer Covariance Matrix

The elements of the jammer covariance, $q_{ln}^{(j)}$, are composed of the expectation of jammer signals

$$q_{ln}^{(j)} = \sum_{j=1}^{J} E\left\{c_{im}c_{kp}^{*}\right\},$$ (2.58)

where m and p are the pulses, i and k are the sensors that expectation is being calculated and J is the number of jammers. It is assumed that jammer signals are temporally uncorrelated and mutually independent. In light of these descriptions using eq. (2.39) in eq. (2.58), jammer covariance matrix element becomes

$$q_{ln} = \begin{cases} \sum_{j=1}^{J} P_j \exp\left[j\frac{2\pi}{\lambda}\left(\left((x_i - x_k)\cos\varphi_j + (y_i - y_k)\sin\varphi_j\right)\cos\theta_j - (z_i - z_k)\sin\theta_j\right)\right] & m = p \\ 0 & m \neq p \end{cases}$$ (2.59)

where ndices l, n, i, k, m, p are defined in eq. (2.49). The calculated jammer covariance matrix

is shown in Figure 2.16
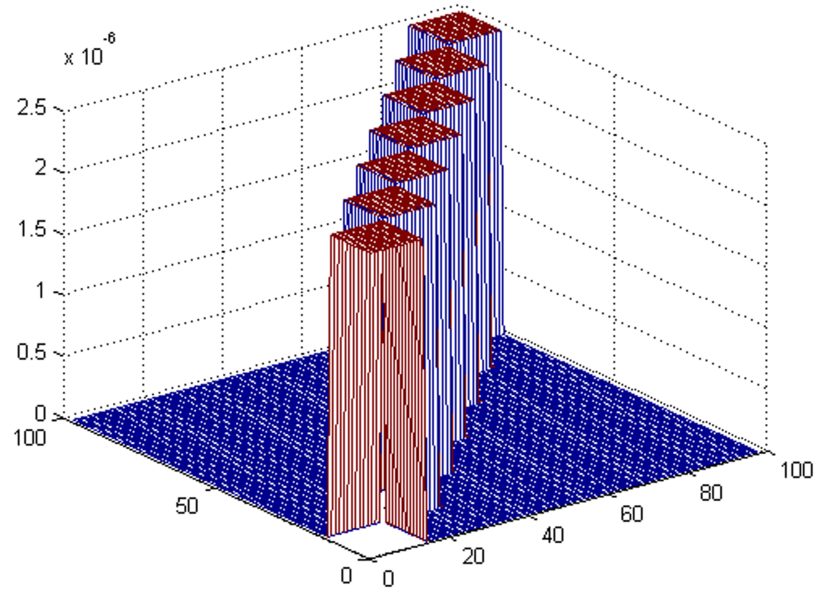
Figure 2.16: Jammer covariance matrix for M=7 and N=14.

2.4.6.4 Noise Covariance Matrix

Noise covariance matrix, Q_n, is calculated by taking the expectation of the noise vector given in eq. (2.40)

$$Q_n = E\left\{\mathbf{n}\mathbf{n}^{\mathrm{H}}\right\} \tag{2.60}$$

Thermal noise (unintentional noise) is uncorrelated in both time and space. Therefore, Q_n given in eq. (2.60) does not have any cross terms is an $NM \times NM$ diagonal matrix scaled by its power as given by

$$Q_n = P_n \mathbf{I}. \tag{2.61}$$

CHAPTER 3

COVERAGE AREA ANALYSIS

Coverage Area Analysis is an operational research area that is used to estimate the strong and weak sides of an electronic defence system. This analysis is being done through calculating the probability of detection for every cell in a study area. Study area is defined according to the analysis needs whether testing the electronic defence systems' vulnerability with respect to the altitude of the incoming target or the azimuth of the incoming target for a selected range interval. Frequently used coverage area programs define the two dimensional study area by picking the two of the variables height, range and azimuth. A couple of frequently used coverage area program outputs are given in Figure 3.1 and Figure 3.2 [20, 21].

In this chapter, basic propagation properties and the degrading effects exerted on electromagnetic wave through propagating path are considered. (This chapter is intended to show that coverage area analysis is being used in real life radar researches.)

The coverage diagram of CARPET shown in Figure 3.1 demonstrates an effect of multipath and coverage diagram of AREPS given in Figure 3.2 demonstrates ducting effect along with multipath.

Mechanism of *multipath* is shown in Figure 3.3 [22] and the reasoning behind this condition can be explained in two items

- Sidelobes of the radiation pattern of antenna.

- Reflective structure of ground.

Now, the lobing effect seen in Figure 3.1 and Figure 3.2 can readily be understood that it is originated from multipath and extra distance traveled by electromagnetic wave through
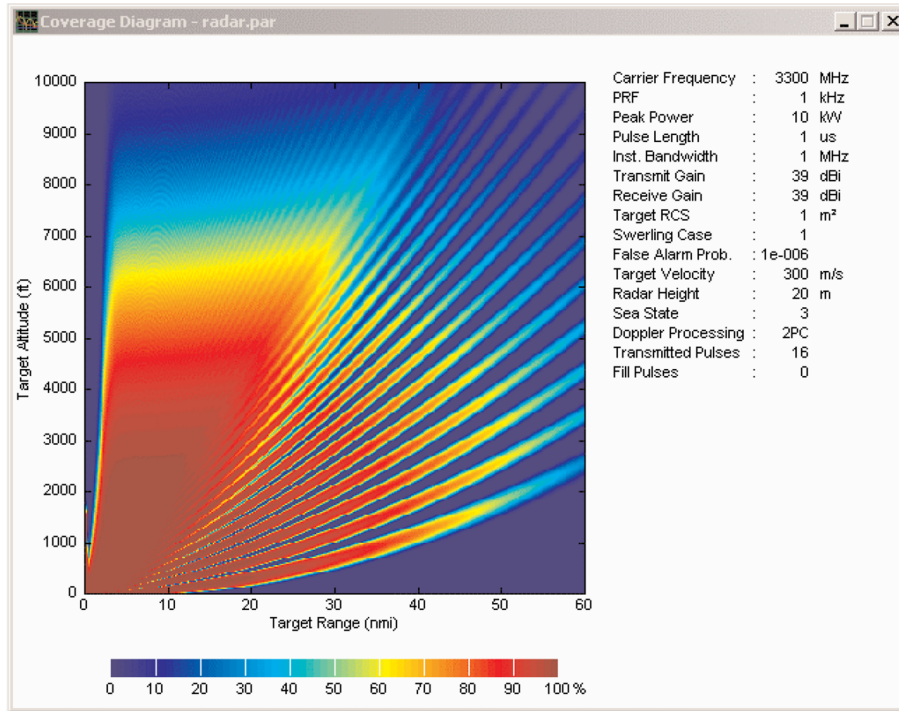
Figure 3.1: Coverage area diagram of CARPET (Computer-Aided Radar Performance Evaluation Tool).
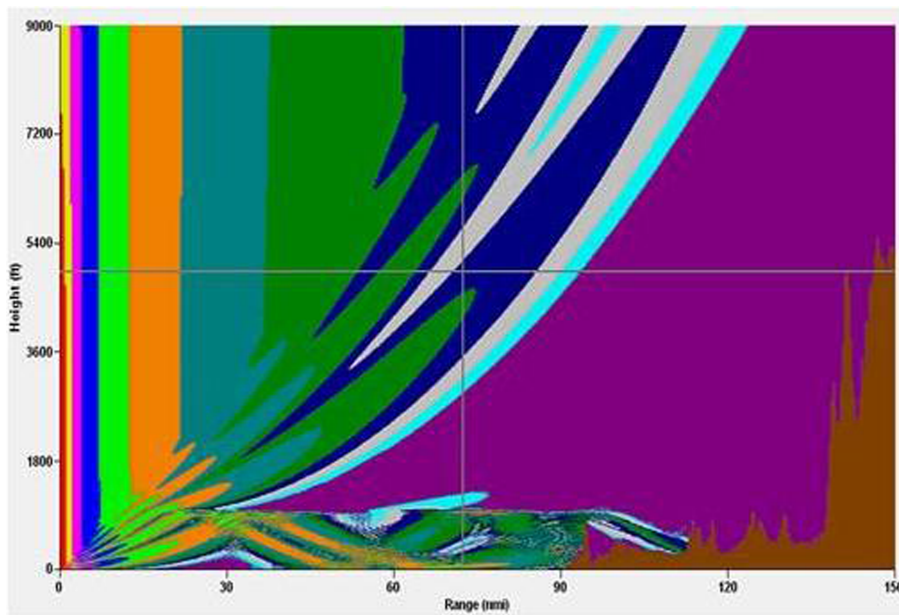

Figure 3.2: Coverage area diagram of AREPS (Advanced Refractive Effects Prediction System).

secondary path.
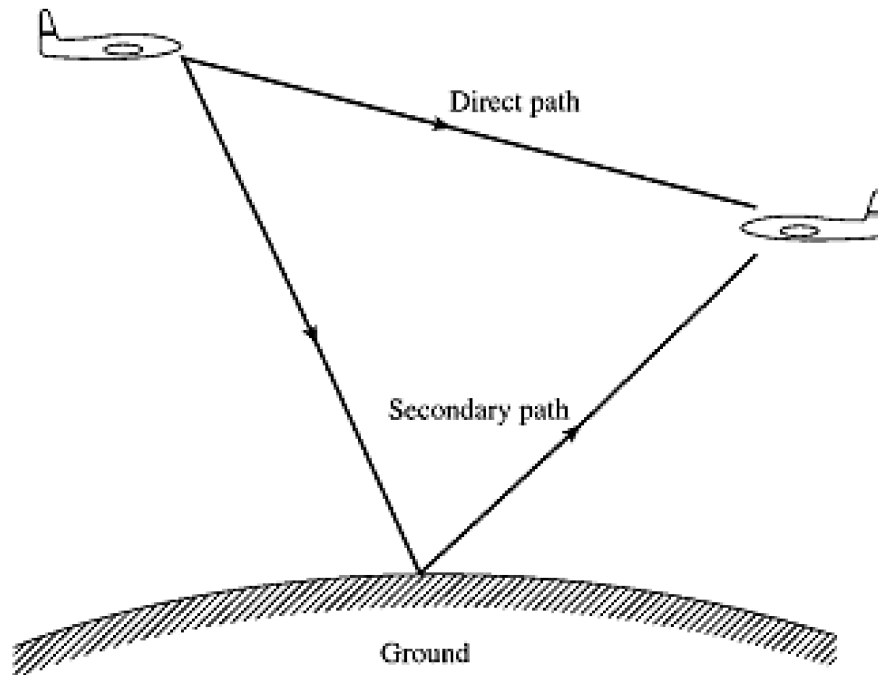
Figure 3.3: Mechanism of multipath.

Up to now, basic propagation effects such as multipath and ducting are presented in this chapter. Chapter will conclude with the explanation of the two of the dominant attenuations (atmospheric attenuation and rain attenuation) that are exerted on the propagating wave.

3.1 Atmospheric Attenuation

Electromagnetic radiation is absorbed by atmosphere due to the interaction of this radiation with molecular dipole moments. Annex-2 of [23] is used in order to predict *atmospheric attenuation*. Annex-2 is bounded by 350 GHz and below 350 GHz, major atmospheric gases that need to be considered are water vapor and dry air (oxygen, pressure-induced nitrogen and non-resonant Debye attenuation). Calculated specific attenuations of dry air and water vapor for pressure 1013hPa temperature $15°C$ and water vapor density $7.5g/m^3$ are shown in Figure 3.4. For further details refer to [23].
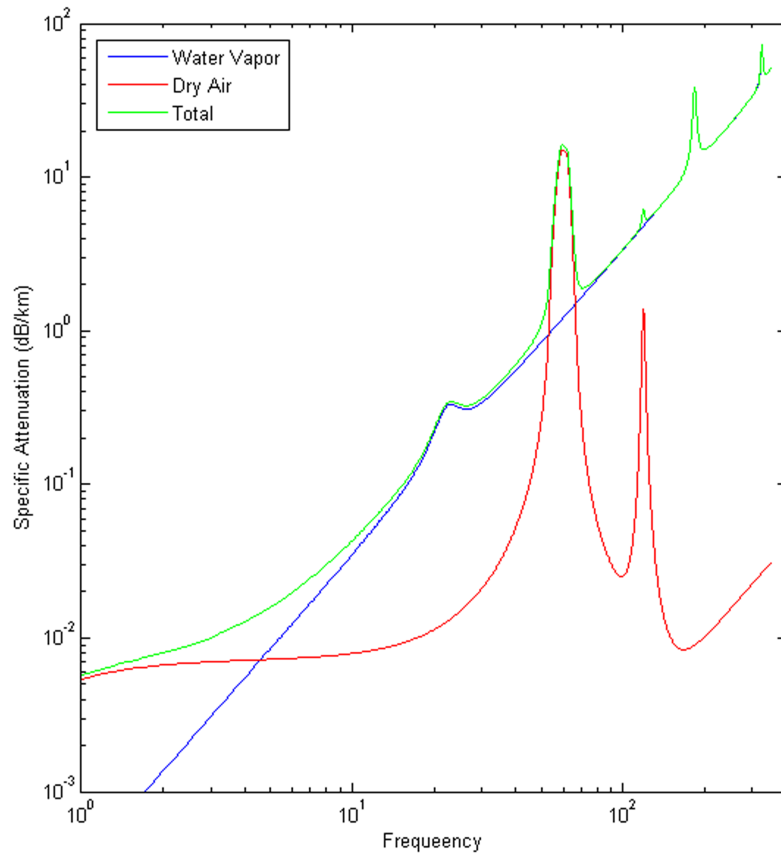
Figure 3.4: Specific attenuation due to atmospheric gases.

3.1.1 Path Attenuation

Signal power decrease due to specific attenuations (γ_0, γ_w are specific attenuations for specific dry air attenuation and specific water vapor attenuation, respectively) are calculated as it is given in [23].

3.1.2 Terrestrial Paths

In this section, atmospheric attenuation for horizontal or slightly inclined paths are estimated. It is called terrestrial because it is applied to the paths close to ground. Loss due to atmospheric attenuation may be written as

$$loss = (\gamma_0 + \gamma_w)R \quad dB \tag{3.1}$$

where R is the path length given in *km*.

3.1.3   Slant Paths

In this section, atmospheric attenuation along slant paths is estimated by defining an equivalent heights for dry air and water vapor, h_0 and h_w, respectively. Equivalent heights are calculated using pressure, temperature and water vapor density appropriate to the altitude of interest. These variables are calculated according to [24]. The estimated loss due to atmospheric attenuation can be written as

$$loss = \gamma_0 h_0 + \gamma_w h_w \quad dB \tag{3.2}$$

3.1.4   Inclined Paths

To determine atmospheric attenuation for an inclined path between stations that are placed at h_1 and h_2 respectively, we need to adjust equivalent heights accordingly

$$\begin{aligned} h'_0 &= h_0 \left(e^{-h_1/h_0} - e^{-h_2/h_0} \right) \quad km \\ h'_w &= h_w \left(e^{-h_1/h_w} - e^{-h_2/h_w} \right) \quad km \end{aligned} . \tag{3.3}$$

The total atmospheric loss can be estimated by using h'_0 and h'_w in eq.(3.2).

3.2   Rain Attenuations

The specific rain attenuation γ_R is obtained by using rain rate, *RainRate* (mm/hr), in power law relationship given as

$$\gamma_R = k \times RainRate^{\alpha}. \tag{3.4}$$

33

Values for the coefficients k and α are determined as a function of frequency and the variables in those equations depends on the polarization of the electromagnetic wave as given in [25]

$$\log_{10}k = \left(\sum_{j=1}^{4} a_j \exp\left[-\left(\frac{\log_{10}(f)-b_j}{c_j}\right)^2\right]\right) + m_k\log_{10}(f) + c_k$$
$$\alpha = \left(\sum_{j=1}^{5} a_j \exp\left[-\left(\frac{\log_{10}(f)-b_j}{c_j}\right)^2\right]\right) + m_\alpha\log_{10}(f) + c_\alpha$$

(3.5)

where f is frequency in GHz, k is either k_H or k_V and α is either α_H or α_V.

Table 3.1: Coefficients for k_H.

j	a_j	b_j	c_j	m_k	c_k
1	-5.33980	-0.10008	1.13098		
2	-0.35351	1.26970	0.45400	-0.18961	0.71147
3	-0.23789	0.86036	0.15354		
4	-0.94158	0.64552	0.16817		

Table 3.2: Coefficients for k_V.

j	a_j	b_j	c_j	m_k	c_k
1	-3.80595	0.56934	0.810618		
2	-3.44965	-0.22911	0.51059	-0.16398	0.63297
3	-0.39902	0.73042	0.11899		
4	0.50167	1.07319	0.27195		

Table 3.3: Coefficients for α_H.

j	a_j	b_j	c_j	m_α	c_α
1	-0.14318	1.82442	-0.55187		
2	0.29591	0.77564	0.19822		
3	0.32177	0.63773	0.13164	0.67849	-1.95537
4	-5.37610	-0.96230	1.47828		
5	16.1721	-3.29980	3.43990		

Table 3.4: Coefficients for α_V.

j	a_j	b_j	c_j	m_α	c_α
1	-0.07771	2.33840	-0.76284		
2	0.56727	0.95545	0.54039		
3	-0.20238	1.14520	0.26809	-0.053739	0.83433
4	-48.2991	0.791669	0.116226		
5	48.5833	0.791459	0.116479		

CHAPTER 4

SPACE-TIME ADAPTIVE SIGNAL PROCESSING

In this chapter, space-time adaptive signal processing methods are described. The simulation results obtained using these methods are given in the next chapter.

It is assumed that sensor array that is used for transmission does not have any back lobes. Simulations throughout this thesis will be done for sidelooking array configuration. Simulated signals will arrive from 0° to 180°.

4.1 Received Signal Processing

This section will concentrate on two *fully adaptive* space-time adaptive processors, namely *Optimum Adaptive Processor* and *Orthogonal Projection Processor*. Adaptive means that the interference cancelation is based on the received interference i.e., the filter weight is calculated from the collected signals at each sensor during one coherent processing interval. For processing purposes it is assumed that

- Interference and desired signals are statistically independent.

- Interference signals are wide-sense stationary.

4.2 Optimum Adaptive Processing

Optimum adaptive space-time adaptive processing for airborne radar is first proposed in [26] and is an extension of *FIR Wiener Processing* [17] to a two dimensional space-time problem. Optimum adaptive processor is given as [13, 14, 27]

$$\mathbf{w} = \gamma \mathbf{Q}^{-1}\mathbf{s}, \tag{4.1}$$

where $\mathbf{Q}$ is the interference+noise covariance matrix $\mathbf{Q} = E\{\chi_i\chi_i^{\mathrm{H}}\}$, where χ defines the interference+noise signal only and $\mathbf{s}$ is the desired signal for the intended weight vector. Block diagram of this optimum processor is shown in Figure 4.1. Antenna elements provides the spatial domain sampling of space-time processor and temporal dimension of space-time processor is provided by the shift registers to store every pulse received during one pulse burst.
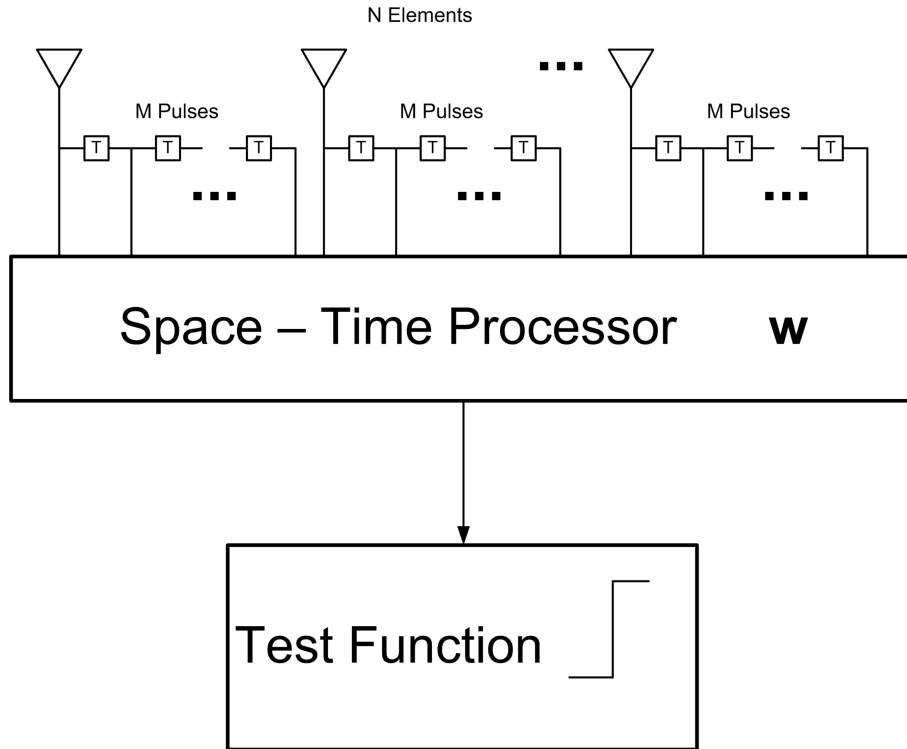

Figure 4.1: Block diagram of optimum adaptive processor.

Test function shown in Figure 4.1 is basically decides whether the output signal contains target signal or just an interference signal. Test function is shown in eq. (4.2).

$$\max_{m} \left| \mathbf{x}^H \mathbf{Q}^{-1}\mathbf{s}_m \right| \begin{cases} > \eta & : \quad \text{Target} + \text{Noise} \\ < \eta & : \quad \text{Noiseonly} \end{cases} \tag{4.2}$$

In eq. (4.2) $\mathbf{x}$ is the received signal, η is the threshold value for the processor and $\mathbf{Q}^{-1}\mathbf{s}_m$ is the weight vector give in eq. (4.1). The effectiveness of any processor over interference can

36

be determined by the improvement factor, IF, [2] - [9] which is defined as the ratio of the output signal-to-noise ratio to the input signal-to-noise ratio.

$$IF = \frac{SINR_{out}}{SINR_{in}} = \frac{\frac{P_s^{out}}{P_{int}^{out}}}{\frac{P_s^{in}}{P_{int}^{in}}} \tag{4.3}$$

Improvement factor given in eq. (4.3) can be represented in matrix form as

$$IF = \frac{SINR_{out}}{SINR_{in}} = \frac{\frac{\mathbf{w}^H \mathbf{s}\mathbf{s}^H \mathbf{w}}{\mathbf{w}^H \mathbf{Q}\mathbf{w}}}{\frac{\mathbf{s}^H \mathbf{s}}{tr(\mathbf{Q})}} \tag{4.4}$$

Improvement factor graphics given in this chapter is normalized to its maximum. Therefore, the maximum value of improvement factor is $0dB$.
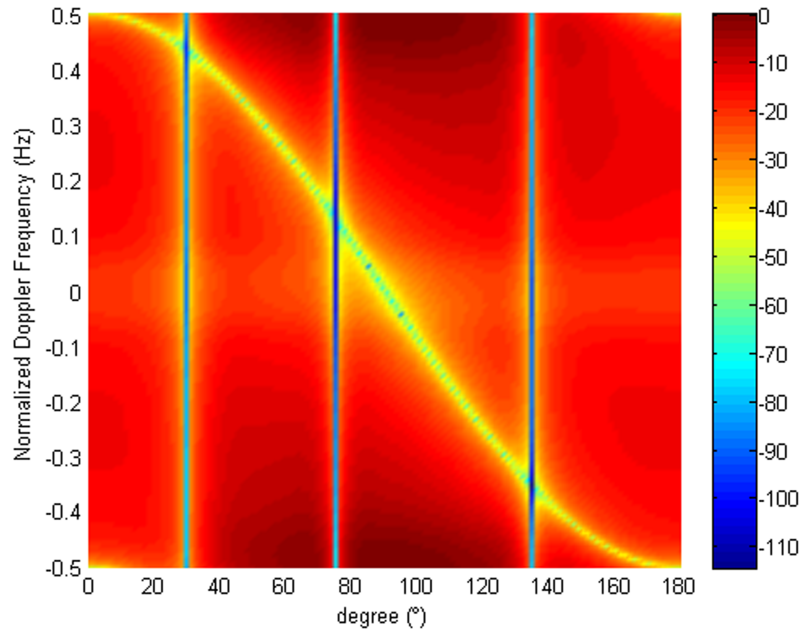

Figure 4.2: Improvement factor of Optimum Adaptive Processor for sidelooking array with three jammers.

Improvement factor of the optimum adaptive processor for sidelooking array is given in Figure 4.2, while that of forward-looking array is in Figure 4.3. There exist three noise jammers. These results are obtained with the same clutter properties given in Figure 2.14. Notice that the difference in Figure 4.3 is due to the array orientation with respect to the displacement

37

vector.
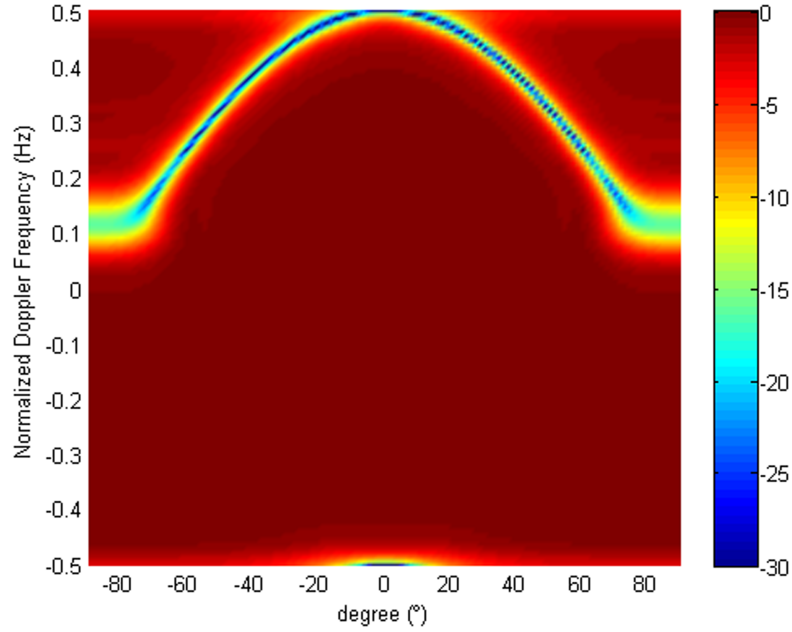
Figure 4.3: Improvement factor of Optimum Adaptive Processor for forward-looking array.

4.3   Orthogonal Projection Processor

Orthogonal projection processor intends to make the interference sources zero whilst optimum adaptive processor tries to maximize the signal-to-noise ratio. Orthogonal projection is based on the eigenvalue decomposition of the interference plus noise covariance matrix. Interference plus noise signal is defined as

$$\mathbf{e}(t) = \mathbf{i}(t) + \mathbf{n}(t), \qquad (4.5)$$

where $\mathbf{i}(t)$ defines the interference signal vector and $\mathbf{n}(t)$ defines the noise vector. Covariance matrix of the interference signal is calculated by using the expectation operator given in eq (4.6).

$$\mathbf{R_e} = E\left\{\mathbf{e}(t)\,\mathbf{e}^{\mathrm{H}}(t)\right\}. \qquad (4.6)$$

Interference plus noise covariance matrix, $\mathbf{R_e}$, can be expressed by its eigenvalues and eigenvectors as

$$\mathbf{R_e} = \mathbf{E}\Lambda\mathbf{E}^{\mathrm{H}}, \tag{4.7}$$

where matrices $\mathbf{E}$ and Λ contains eigenvectors and eigenvalues of $\mathbf{R_e}$, respectively. We know that eigenvectors in $\mathbf{E}$ are orthogonal to each other. It is assumed that eigenvalues of interference and noise can be separated. Therefore, by using the separated eigenvalues of noise and interference and corresponding eigenvectors eq. (4.7) can be separated as

$$\mathbf{R_e} = \mathbf{E}^{(i)}\Lambda^{(i)}\left(\mathbf{E}^{(i)}\right)^{\mathrm{H}} + \mathbf{E}^{(n)}\Lambda^{(n)}\left(\mathbf{E}^{(n)}\right)^{\mathrm{H}}, \tag{4.8}$$

where n and i defines noise and interference, respectively.

Therefore, projection operator that is orthogonal to interference subspace is given as

$$\mathbf{P} = \mathbf{I} - \mathbf{E}^{(i)}\left(\left(\mathbf{E}^{(i)}\right)^{\mathrm{H}}\mathbf{E}^{(i)}\right)^{-1}\left(\mathbf{E}^{(i)}\right)^{\mathrm{H}}, \tag{4.9}$$

The weight vector of orthogonal projection processor is given as

$$\mathbf{w} = \mathbf{Ps}, \tag{4.10}$$

where $\mathbf{s}$ is the desired signal [28]. The improvement factor of the orthogonal projection processor is found by using the weight vector, eq. (4.10) in eq. (4.4) as given by

$$IF = \frac{\frac{\mathbf{s}^{\mathrm{H}}\mathbf{P}^{\mathrm{H}}\mathbf{s}\mathbf{s}^{\mathrm{H}}\mathbf{Ps}}{\mathbf{s}^{\mathrm{H}}\mathbf{P}^{\mathrm{H}}\mathbf{QPs}}}{\frac{\mathbf{s}^{H}\mathbf{s}}{tr(\mathbf{Q})}} = \frac{\mathbf{s}^{\mathrm{H}}\mathbf{P}^{\mathrm{H}}\mathbf{s}\mathbf{s}^{\mathrm{H}}\mathbf{Ps} \times tr(\mathbf{Q})}{\mathbf{s}^{\mathrm{H}}\mathbf{P}^{\mathrm{H}}\mathbf{QPs} \times \mathbf{s}^{H}\mathbf{s}}. \tag{4.11}$$

The only difference between the orthogonal projection processor and the optimum adaptive processor is the usage of the *projection opeartor* instead of the interference plus noise covariance matrix in the block diagram given in Figure 4.1

The improvement factors obtained from the orthogonal projection processor and the optimum adaptive processor is compared in Figure 4.4.
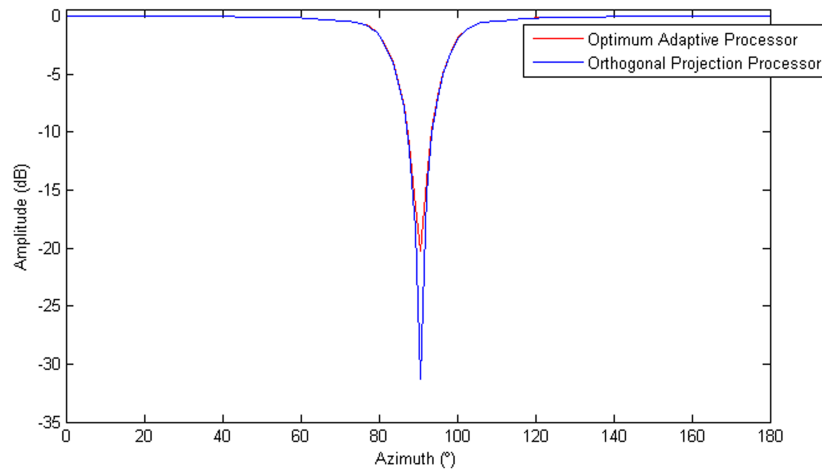
Figure 4.4: IF's of the orthogonal and optimum adaptive processor.

As we can observe from Figure 4.4, the orthogonal projection processor displays deeper notch than the optimum adaptive processor. This is the direct consequence of projection of the desired signal onto the space that is orthogonal to the interference space.

4.4 Effects of Radar Parameters on Interference Cancelation

In this section, influence of radar parameters on interference cancelation is discussed.

4.4.1 Effects of Array and Sample Size

In one dimensional signal processing (spatial or temporal), number of samples taken from a continuous signal directly affects the resolution of the frequency spectrum. As the number of sensors in an array or the number of transmitted pulses increases, the resolution of spatial spectrum or temporal spectrum increases. This is illustrated for a sidelooking array by changing the number of sensors in Figure 4.5

Figure 4.5 is plotted for $45°$ azimuth angle. As we can observe from Figure 4.5, we can make the notch narrower by increasing the number of sensors in the array. Increasing resolution in one dimension will not effect the resolution of the other dimension. Therefore, the clutter resolution is limited by the smaller of the number of sensors and the number of pulses. We
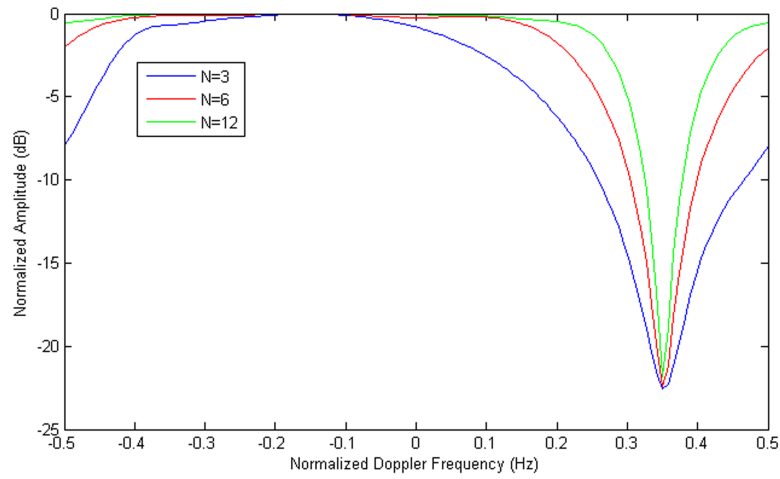
Figure 4.5: Effect of array size for sidelooking array.

can see this situation by comparing Figure 4.6 and Figure 4.7. As we can observe the notch in Figure 4.7 is narrower than the notch in Figure 4.6.
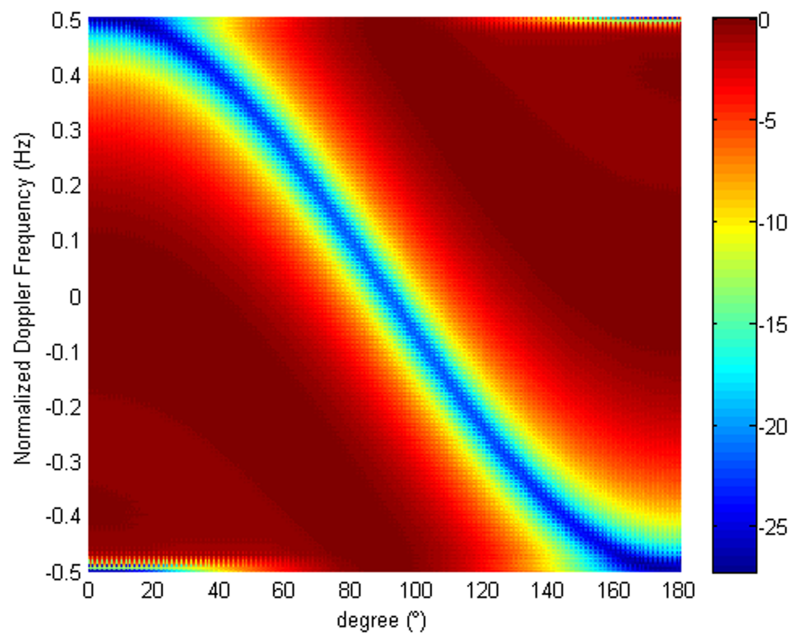

Figure 4.6: Improvement factor of the optimum adaptive processor with N=3 and M=48.
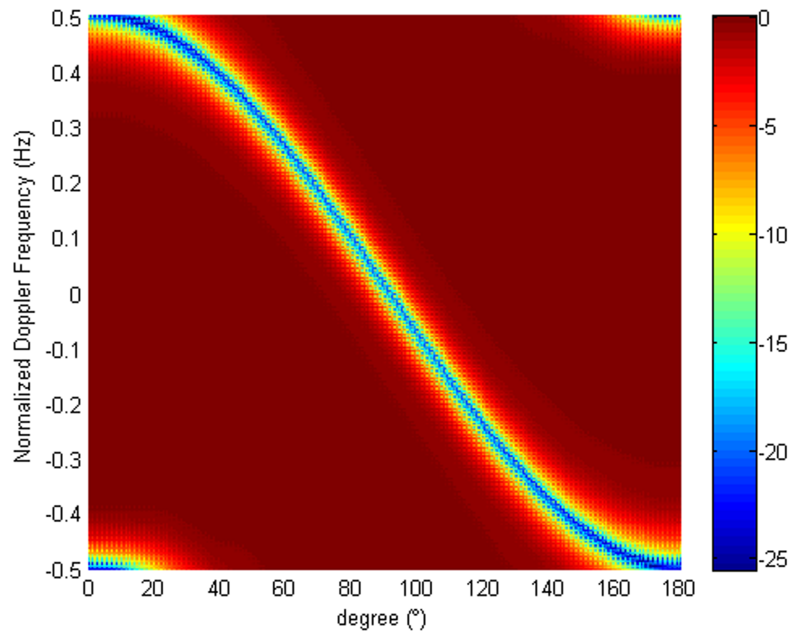
Figure 4.7: Improvement factor of the optimum adaptive processor with N=12 and M=12.

4.4.2 Sampling Effects

This section describes the effects of the sampling in spatial and temporal domains on the processing performance.

The sampling in the temporal domain is done by the received pulses, that is the sampling period is PRI (or the sampling frequency is PRF). The Doppler frequency above the PRF are ambiguous. Depending of the PRF value and the frequency spread of the stationary clutter, which is due to the platform motion, there may be ambiguity in temporal domain. This situation corresponds to the temporal undersampling which results in a case shown in Figure 4.8 for sidelooking array with PRF is $6kHz$ and velocity of the platform, v_p, is $90m/s$.

PRI determines the temporal sampling while the intersensor distance determines the spatial sampling. Undersampling is spatial domain may result in aliasing as shown in Figure 4.9 for a forward-looking array with intersensor displacement, d, equal to λ.
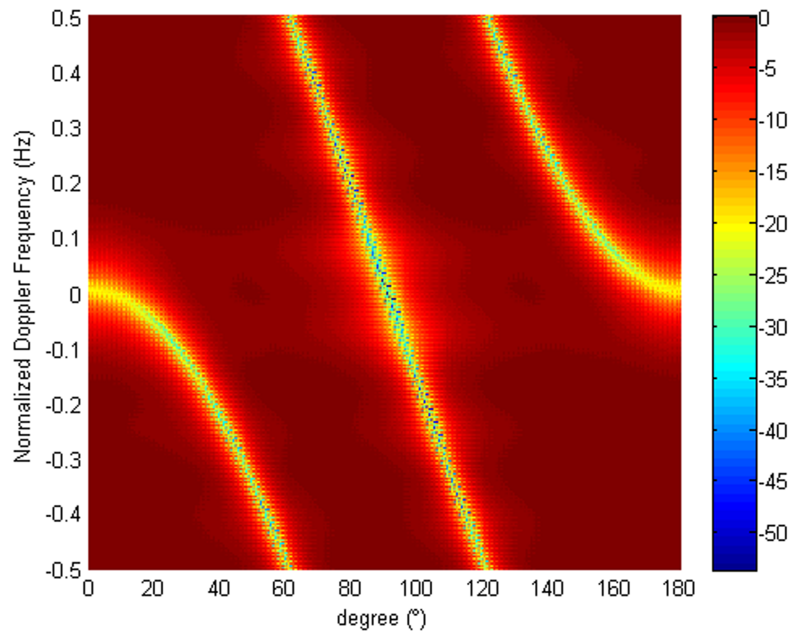
Figure 4.8: Improvement factor for temporal undersampling, PRF=6kHz and $v_p = 90$m/s.
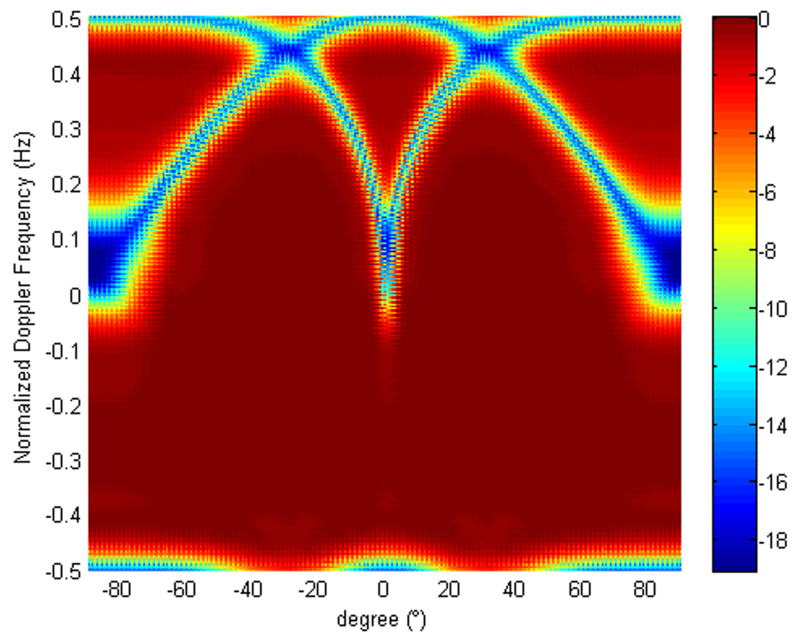
Figure 4.9: Improvement factor for spatial undersampling, $d = \lambda$.

4.4.3 Clutter Bandwidth

Clutter bandwidth is a direct consequence of internal clutter motion. This is called as temporal decorrelation in 2.4.6.2. Internal clutter motion widens the clutter notch of the processor. Hence, this will affect the detection of slowly moving targets. This situation is shown in Figure 4.10 for different normalized clutter fluctuation bandwidth, $B_c = 2\sigma/PRF$. Figure 4.10 shows one slice of the improvement factor for 45° azimuth. As we can observe from Figure 4.10, widened clutter notch will degrade the detection of potential slowly moving targets.
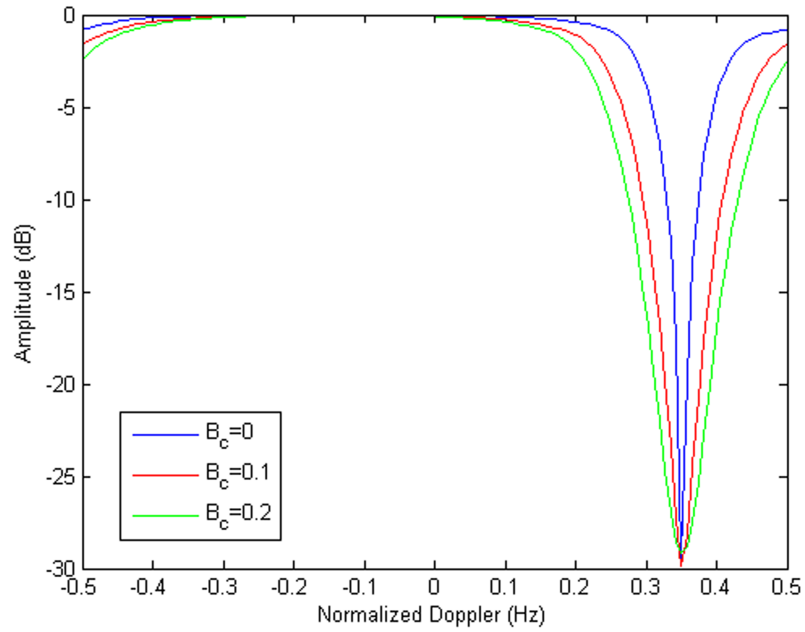

Figure 4.10: The influence of the internal clutter motion.

4.5 Filtering Process

The calculated weight vector response, which is a function of angle and Doppler, is an indicator of the performance of the processor. This response is called the *adapted pattern* given as

$$AdaptedPattern\,(\varphi, f_D) = \left| \mathbf{w}^{\mathrm{H}} \mathbf{v}\,(\varphi, f_D) \right|^2, \tag{4.12}$$

44

where **w** is the weight vector of the processor and **v** is the vector that represents the signal at φ and f_D. For a uniform linear array and fixed pulse repetition interval, the adapted pattern corresponds to the two dimensional Fourier transform of the weight vector. In the absence of interference, the adapted pattern is called as *quiescent pattern*. Quiescent adapted pattern of optimum adaptive processor is shown in Figure 4.11 [14]. Figure 4.11 is calculated for the target located at 40° azimuth and 0.11 normalized Doppler.
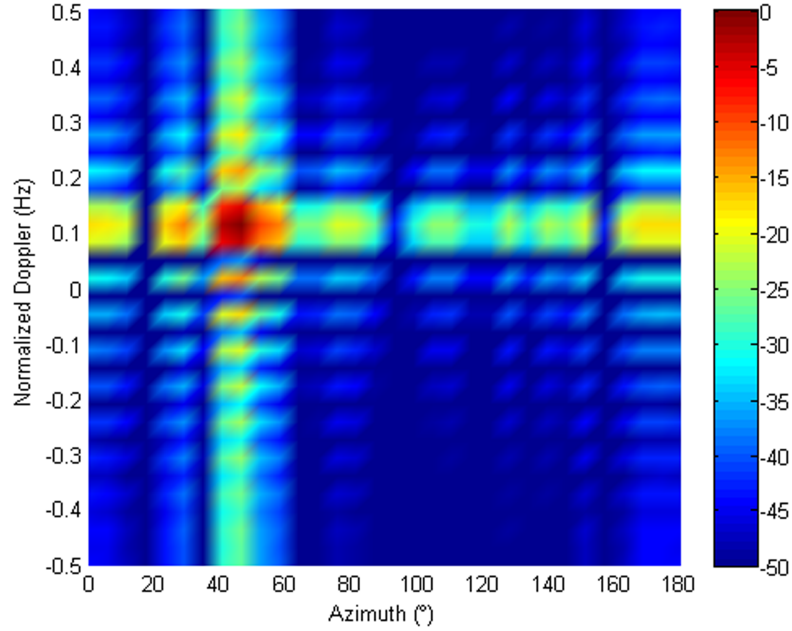

Figure 4.11: Quiescent adapted pattern.

The adapted pattern of the processor for the parameters given in Table 4.1 is shown in Figure 4.12. As we can observe from the Figure 4.12 adapted pattern has nulls in the direction of interference and gain at the azimuth angle and the Doppler frequency of the target.

The applied gain on target can be found as

$$Gain = 10 \log_{10} (M \times N),\tag{4.13}$$

where M is the number of pulses transmitted in one CPI and N is the number of sensors in the array. The adapted pattern figures shown in the next chapter will be normalized with respect to its maximum gain.

Table 4.1: Simulation parameters.

| Platform Parameters	
Height (H)	1000m
Velocity (v_p)	90 m/s
ψ angle	0°
Number of sensors (N)	16
Target Parameters	
Range	10km
Azimuth	40°
Relative Velocity (v_{rad})	20m/s
Radar Cross Section (RCS)	$10dBm^2$
Radar Parameters	
Operating Frequency	10GHz
Peak Power	10kW
Pulse Repetition Frequency (PRF)	12kHz
Duty Cycle	%1
Number Of Pulses (M)	16
Jammer Properties	
Number of Jammers (J)	1
Range	9km
Azimuth	90°
Jammer-To-Noise Ration (JNR)	$90dB$
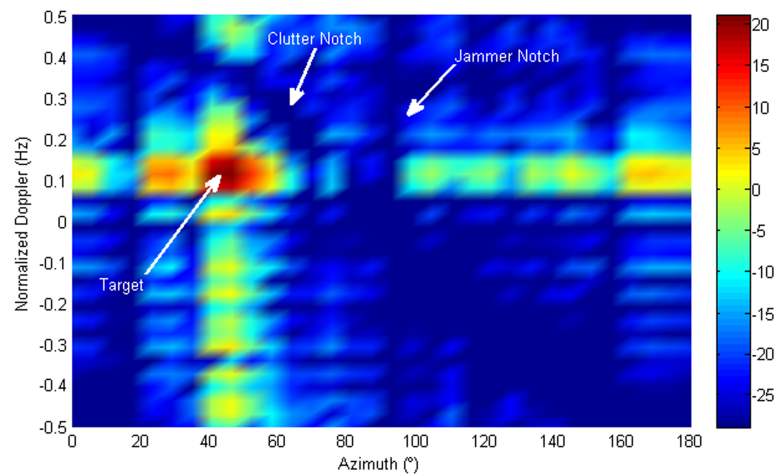
Figure 4.12: Adapted pattern of optimum processor, target at 40° azimuth and 0.11 normalized Doppler frequency.

CHAPTER 5

SIMULATION RESULTS

This chapter gives the simulation results for the optimum adaptive processing technique given in Chapter 4. The simulations start with a landbased radar, where clutter does not exhibit two dimensional spread in azimuth-Doppler plane. Then it will continue for *interference* elimination for airborne radar. Finally, simulations will conclude by using space-time adaptive processing for coverage area purposes.

5.1 Jammer Cancelation for Static Radar

It has been discussed that clutter exhibits two dimensional spread in spatial frequency-Doppler plane due to platform motion. If the radar platform is motionless, than clutter will not exhibit two dimensional spread. Parameters that used in simulations are given in Table 5.1.

Figure 5.1 shows the calculated adapted pattern. We can see that the main lobe of the adapted pattern is located on target's spatial frequency and Doppler frequency. Spatial frequency of the assumed target is given in Table 5.1 and Doppler frequency of the target can be calculated by using radial velocity of the target and operating frequency of the radar in eq. (2.5). By using the notches, interference sources are suppressed.

Figure 5.2 shows the input power spread before the processor. It can be seen that interference powers are well above the target's power.

Figure 5.3 shows the output power spread after the processor. It can be seen that after processing, target signal is ready to be sent to test the function to perform detection.

The color bar range for the processor output figures are calculated with respect to the required

Table 5.1: Simulation parameters.

Platform Parameters	
Height (H)	1000m
Velocity (v_p)	0 m/s
ψ angle	0°
Number of sensors (N)	16
Inter Element Displacement (d)	$\frac{\lambda}{2}$
Target Parameters	
Range	10km
Spatial Frequency	−0.1702
Relative Velocity (v_{rad})	20m/s
Radar Cross Section (RCS)	$10dBm^2$
Radar Parameters	
Operating Frequency	10GHz
Peak Power	10kW
Pulse Repetition Frequency (PRF)	12kHz
Duty Cycle	%1
Number Of Pulses (M)	16
Jammer Properties	
Number of Jammers (J)	1
Range	9km
Spatial Frequency	0.3825
Jammer-To-Noise Ration (JNR)	$90dB$
Clutter Properties	
Sigma Zero (σ_0)	824.3054
Clutter-To-Noise Ration (CNR)	$68.7942dB$

SINR for the detection. Required SINR is calculated as

$$SINR = \left(erfc^{-1}\left(2p_{fa}\right) + erf^{-1}\left(2\left(p_d - 0.5\right)\right)\right)^2, \qquad (5.1)$$

where p_{fa} is the false alarm probability and p_d is the probability of detection [3]. False alarm probability and the probability of detection is assumed as $1e − 6$ and 0.9 for the rest of the simulations.

In order to see the effectiveness of space-time adaptive processor, same simulation will be repeated with one sensor which will be equivalent to temporal processing. The adapted pattern in Figure 5.4 shows that one sensor cannot distinguish the spatial phase differences. Hence, the processor can not discriminate the angle-of-arrivals. Since we can not prepare an anti-jamming filter in spatial domain jammer signal dominates the output signal spectrum as in
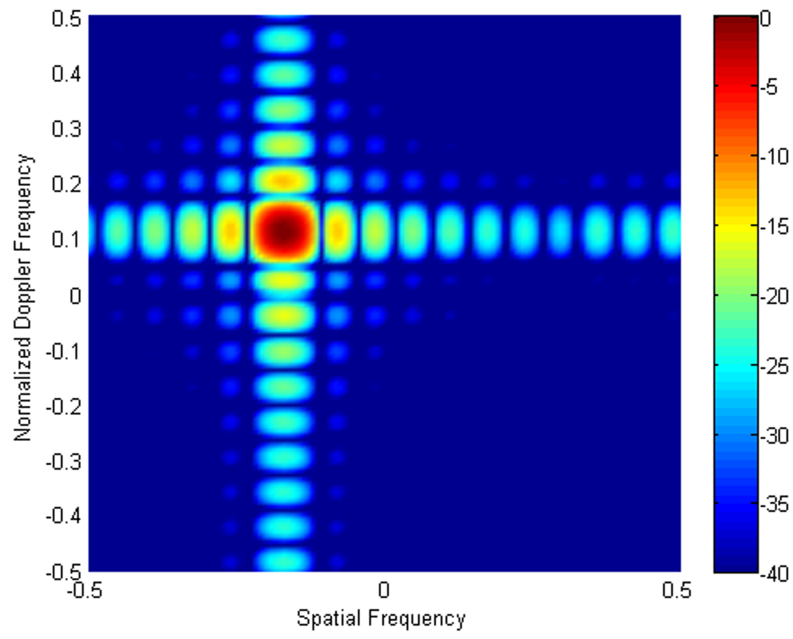
Figure 5.1: Adapted pattern, N=16.
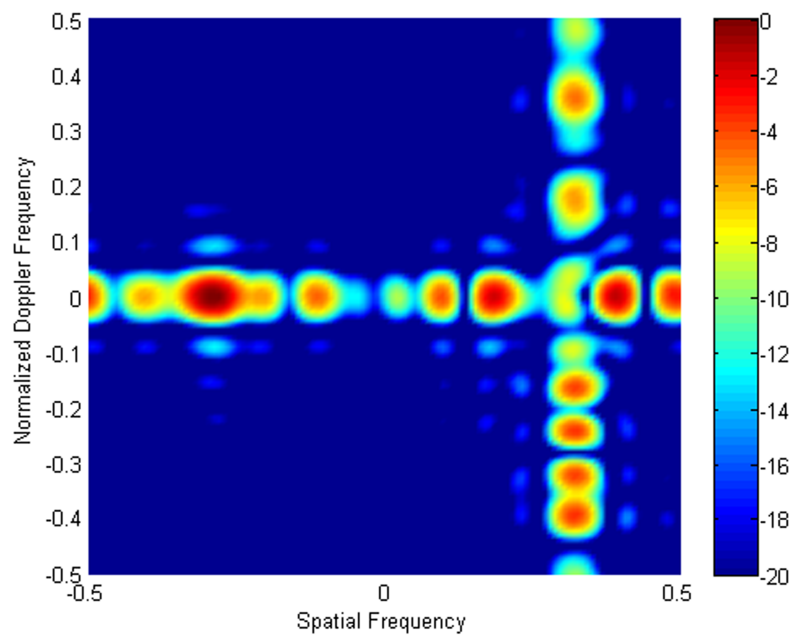
Figure 5.2: Power spread before the processor.
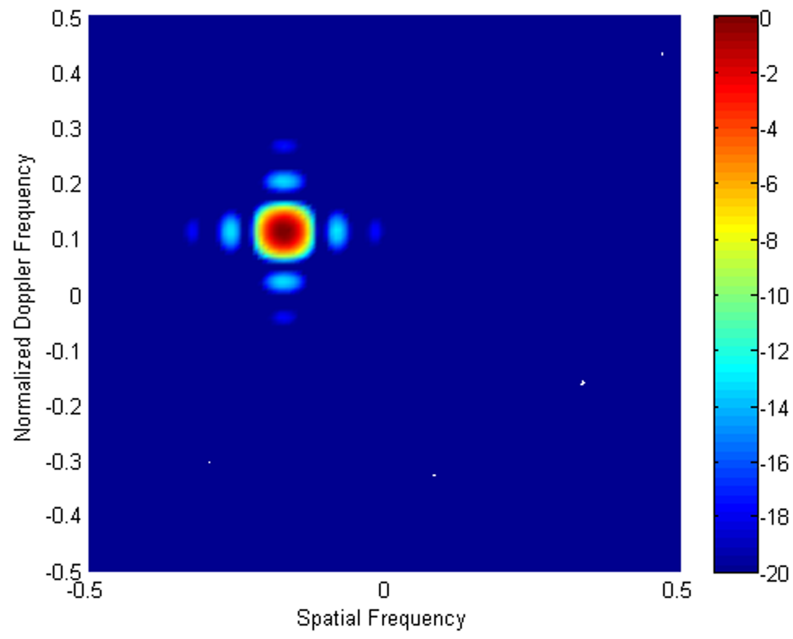
Figure 5.3: Power spread after processor, N=16.

Figure 5.5
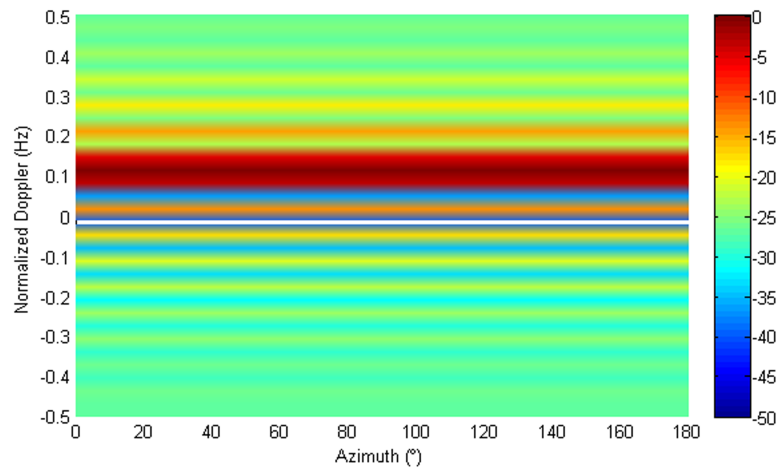
Figure 5.4: Adapted pattern, N=1.
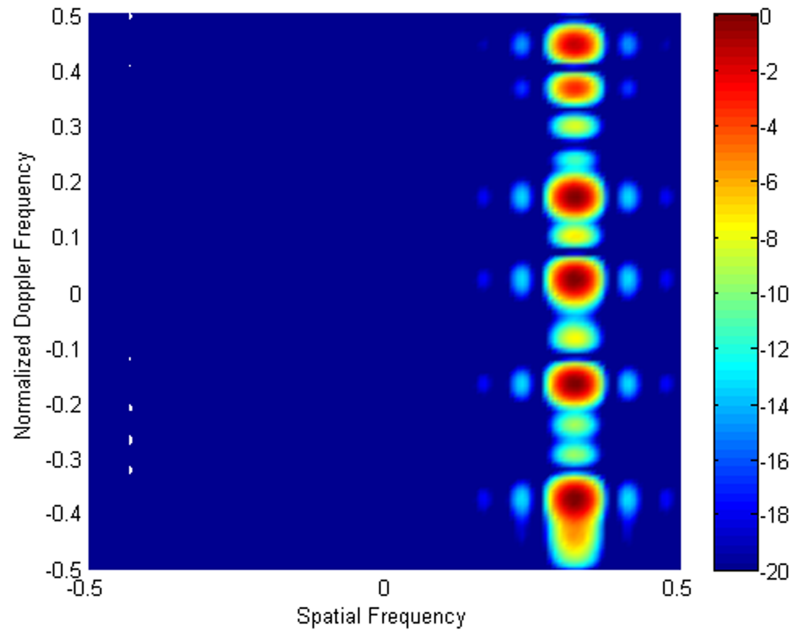
Figure 5.5: Power spread after processor, N=1.

5.2 Interference Cancelation for Airborne Radar

This section concentrates on interference cancelation for airborne radar by using space-time adaptive processing. This section will discuss the effectiveness of space-time adaptive processing processor by changing the simulation parameters. The relation in between the effectiveness of space-time adaptive processing and the simulation parameters is analyzed.

Unlike the static radar, this time we have an airborne radar with platform velocity $90 m/s$ and three jammers located at -0.3210, 0.1708 and 0.3825 spatial frequencies. Since the platform is mobile, clutter will present two dimensional spread in Doppler-spatial frequency plane. The Doppler-spatial frequency plane of processor input is given in Figure 5.6

Interference signals in Figure 5.6 are well above the target signal. However, jammer and clutter signals are eliminated by the notches observed in Figure 5.7. The output of this filtering process is given in Figure 5.8

As it was mentioned before, depending on the radar parameters such as PRF, clutter spread echoes may be undersampled or oversampled. It will be shown that any variation in radar
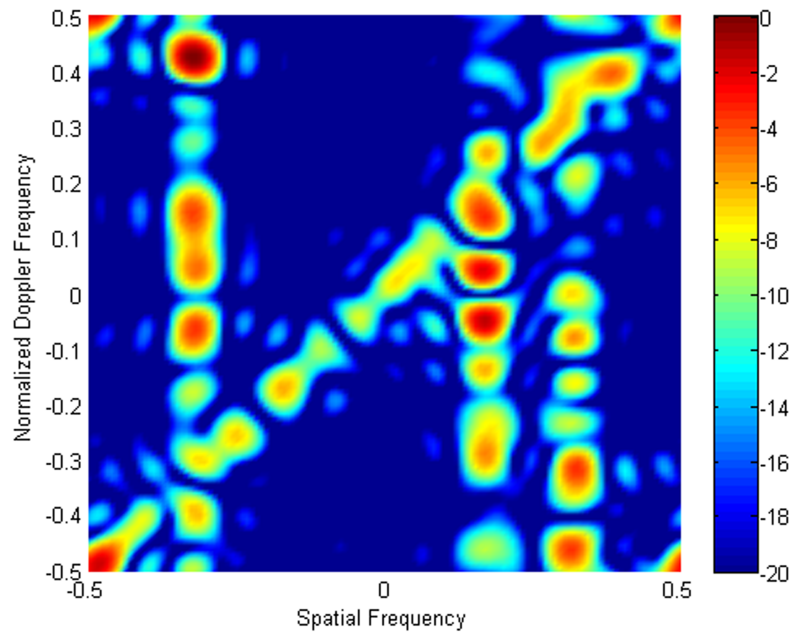
Figure 5.6: Power spread before processor.
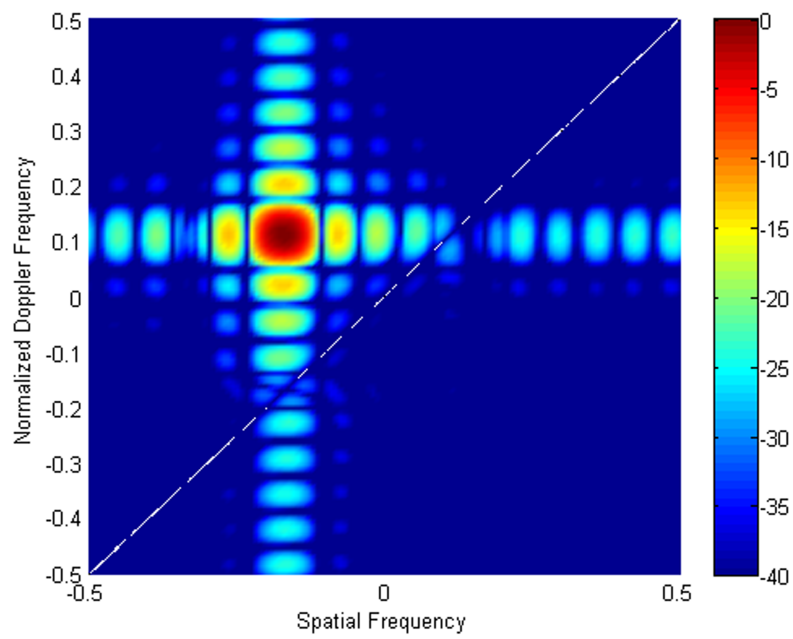

Figure 5.7: Adapted pattern.
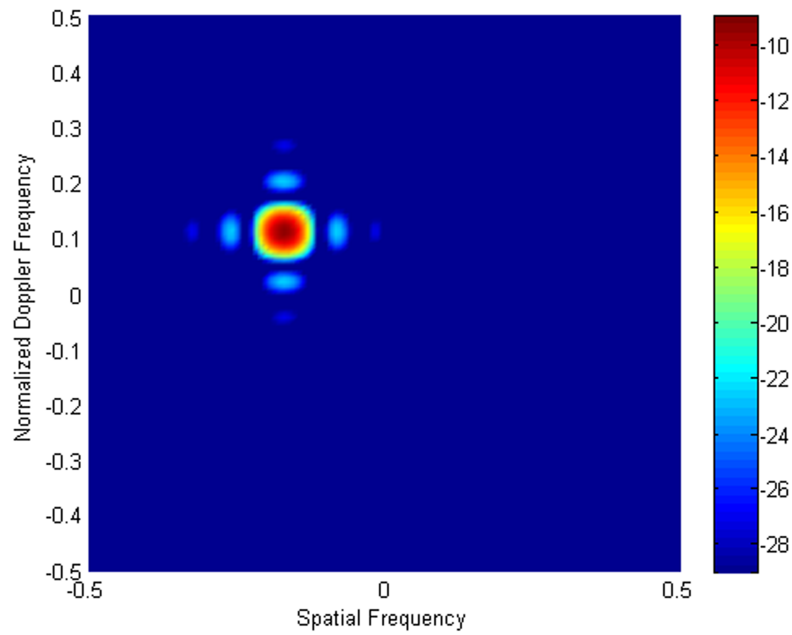
Figure 5.8: Power spread after processor.

parameters will effect the detectability of potential targets. Since clutter spread may be aliased or shrunk along Doppler-spatial frequency domain with respect to these parameters. The input power spread for *PRF* = 6*kHz* is given in Figure 5.9. As it is expected, clutter is aliased due to undersampling in temporal domain. Aliased clutter signal and three jammer signals after space-time adaptive processing are presented in Figure 5.10. The cancelation operation is done via the adapted pattern given in Figure 5.11.

In order to undersample in the spatial domain, the original inter element displacement value is doubled to λ. Input power spread is given in Figure 5.12. Adapted pattern for this situation is given in Figure 5.13.

If the target is placed on the jammer azimuth position (same spatial frequency, -0.1702), then adapted pattern would not be able to discriminate the received signals from target or jammer. This situation is demonstrated from Figure **??** to Figure **??**.

53
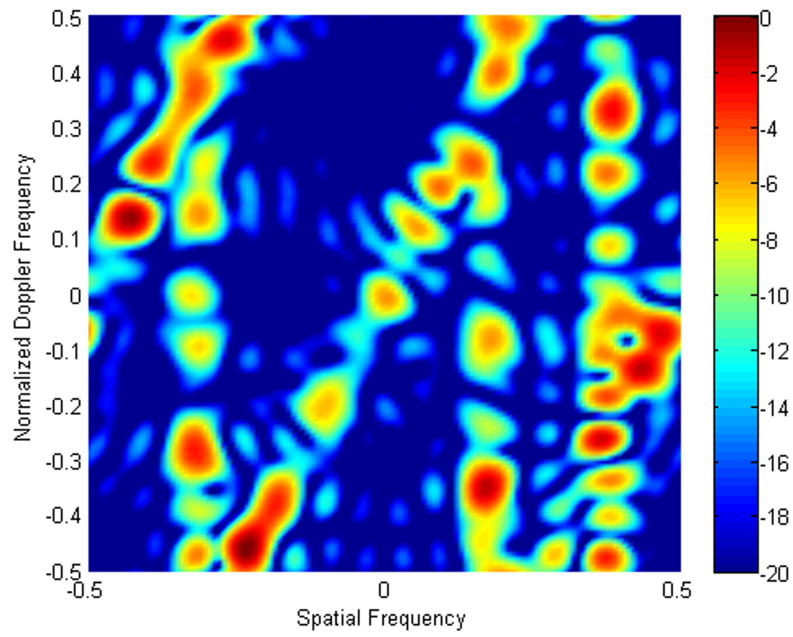
Figure 5.9: Power spread before the processor, PRF=6kHz.
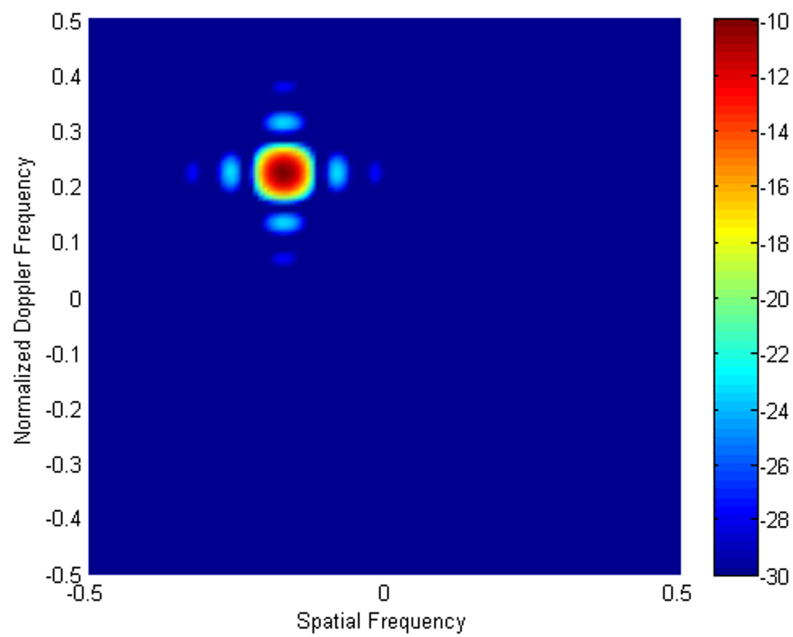

Figure 5.10: Power spread after processor, PRF=6kHz
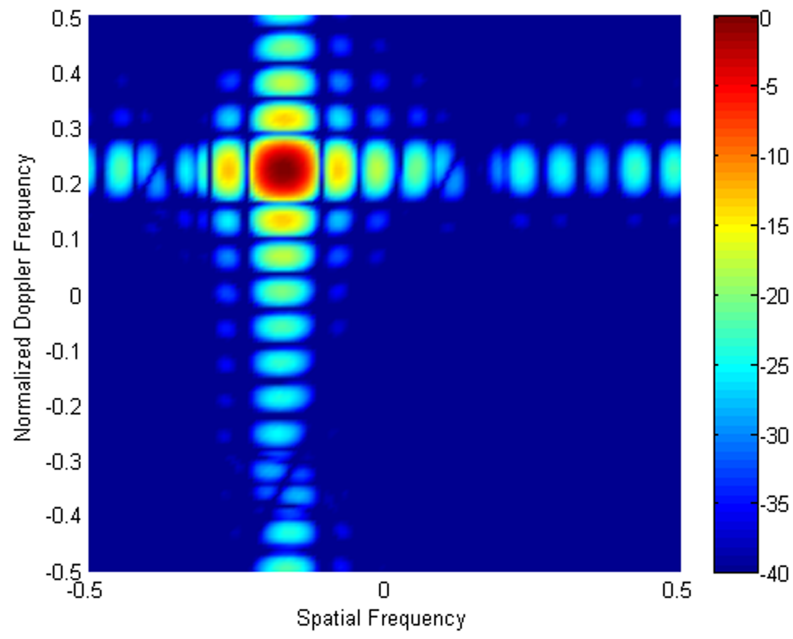
Figure 5.11: Adapted pattern, PRF=6kHz.
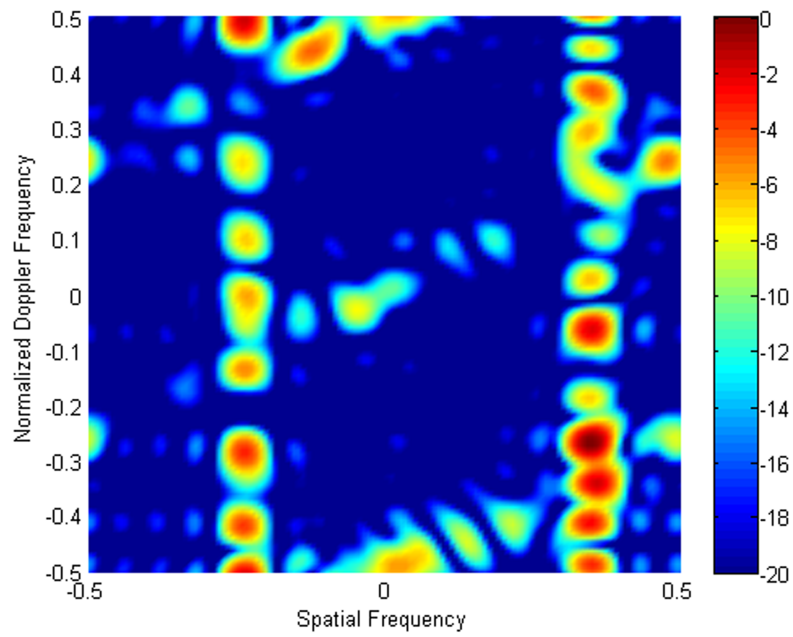
Figure 5.12: Power spread before the processor, d=λ.
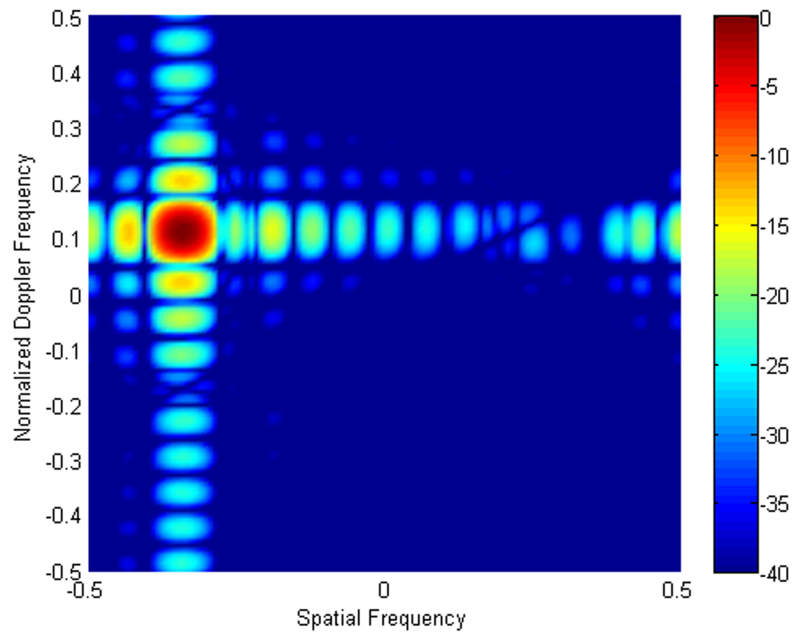
Figure 5.13: Adapted pattern, d=λ.
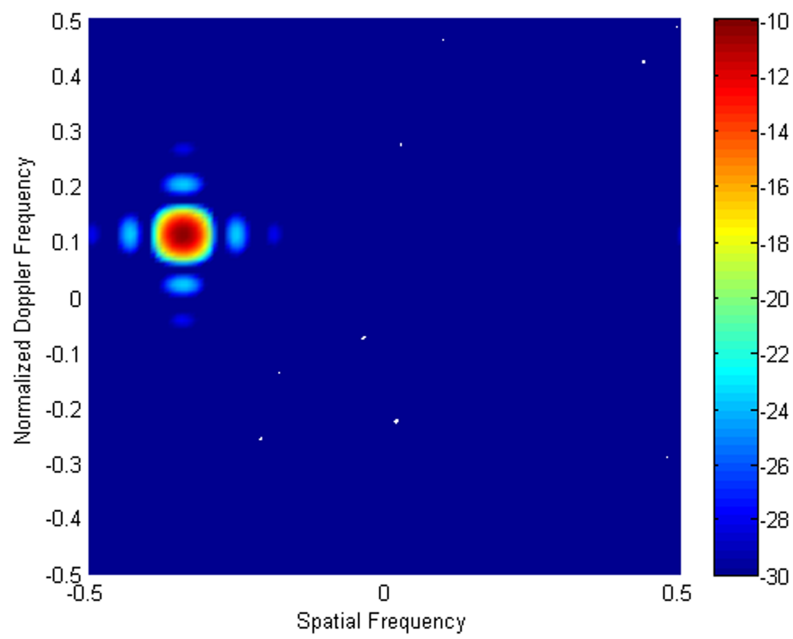
Figure 5.14: Power spread after the processor, d=λ.
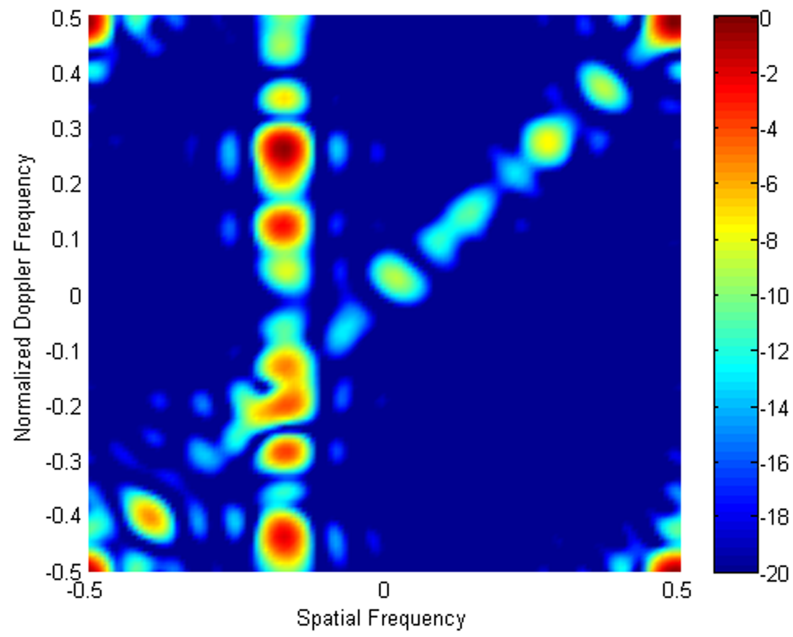
Figure 5.15: Power spread before the processor, target is on the same spatial frequency with jammer.
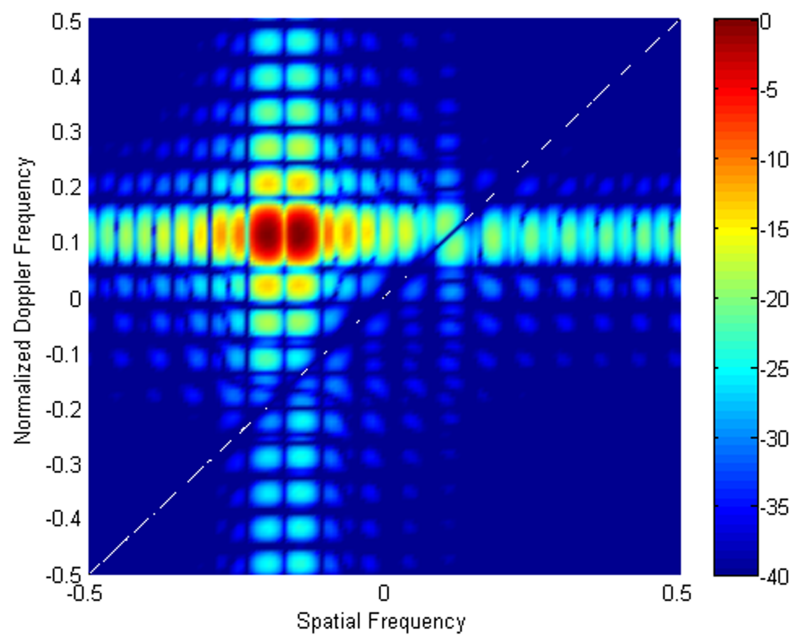

Figure 5.16: Adapted pattern, target is on the same spatial frequency with jammer.
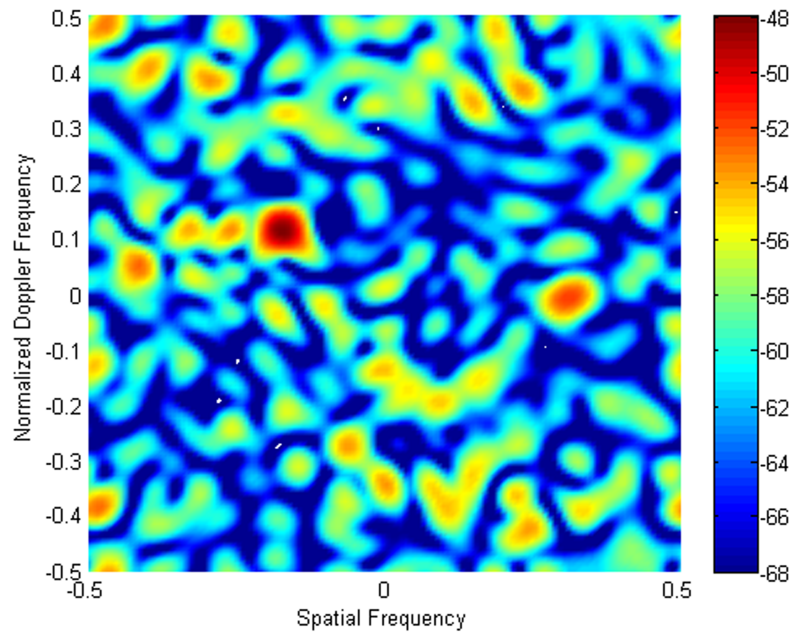
Figure 5.17: Power spread after the processor, target is on the same spatial frequency with jammer.

5.3 Coverage Area Analysis

Coverage area analysis may be used to find weak spots in the hostile or friendly defence line. The effects of space-time adaptive processing in coverage area analysis is provided in this section. The purpose usage of space-time adaptive processing in coverage area analysis is to show the income in detecting potential targets with respect to the traditional signal processing. The simulation parameters are given in Table 5.2.

Coverage area analysis is evaluated via calculating the probability of detection over all Doppler and azimuth spectrum. Therefore, target properties are removed from Table 5.2.

To observe the effectiveness of space-time adaptive processing on coverage area calculations, the coverage area results of the radar systems that employ traditional signal processing tools and space-time adaptive processing is presented.

Coverage area simulation result for the parameters given in Table 5.2 is presented in Figure 5.18.

58

Table 5.2: Coverage area simulation parameters.

Platform Parameters	
Height (H)	1000m
Velocity (v_p)	90 m/s
ψ angle	0°
Number of sensors (N)	9
Inter Element Displacement (d)	$\frac{\lambda}{2}$
Radar Parameters	
Operating Frequency	10GHz
Peak Power	10kW
Pulse Repetition Frequency (PRF)	12kHz
Duty Cycle	%1
Number Of Pulses (M)	9
Jammer Properties	
Number of Jammers (J)	3
Range	9km, 6km, 7km
Azimuth	$15°, 60°, 110°$
Jammer-To-Noise Ration (JNR)	$90dB, 80dB, 110dB$
Clutter Properties	
Sigma Zero (σ_0)	824.3054
Clutter-To-Noise Ration (CNR)	$68.7942dB$

In order to see the effect of the number of transmitted pulses and the number of the sensors in the array, both have been varied between 1 to 9 while keeping the single jammer.

The result of three pulses and one sensor is given in Figure 5.19. As it is expected coverage area analysis does not give any detection due to the clutter spread along Doppler-azimuth space and jamming.

when the number of sensors in the array and the transmitted pulses are increased to four. We obtain Figures 5.18 and 5.20 for the coverage area. As can be observed from these figures the coverage area is increased when the number of sensors in the array and the number of transmitted pulses are increased. This is a direct consequence of the increased resolution due to the increased number of sensors employed in the antenna and the number of pulses transmitted during one CPI. Increasing the coverage area via increasing the number of sensors or number of pulses is presented in Figure 5.20 and Figure 5.21 with jammer located at 15° azimuth.
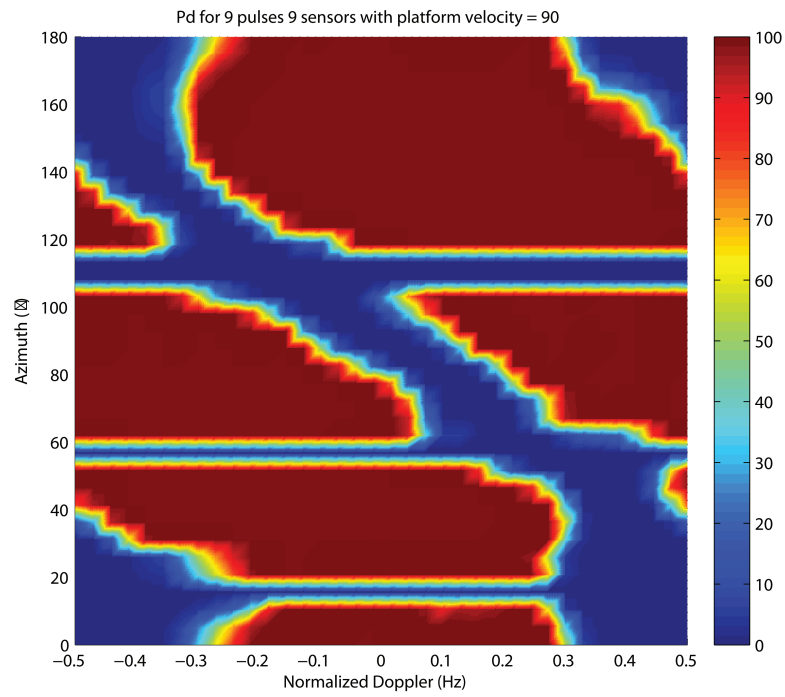
Figure 5.18: Coverage area analysis output, P_d for 9 pulses and 9 sensors.
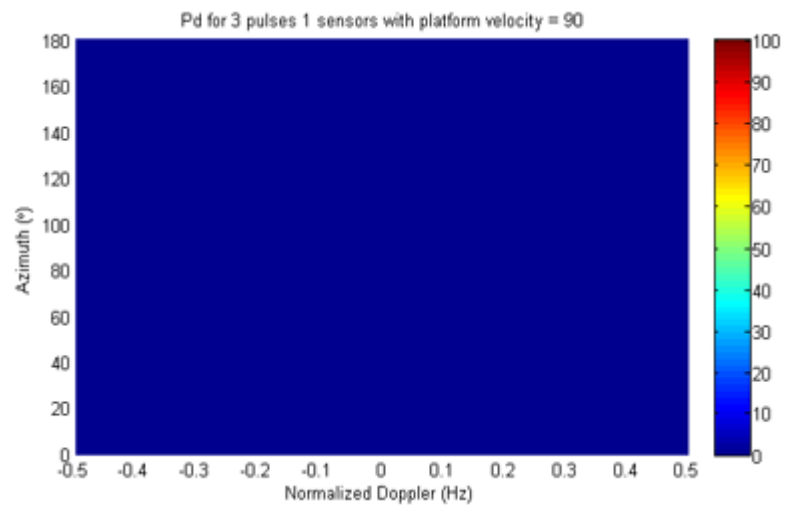

Figure 5.19: Coverage area analysis output, P_d for 3 pulses and 1 sensors.
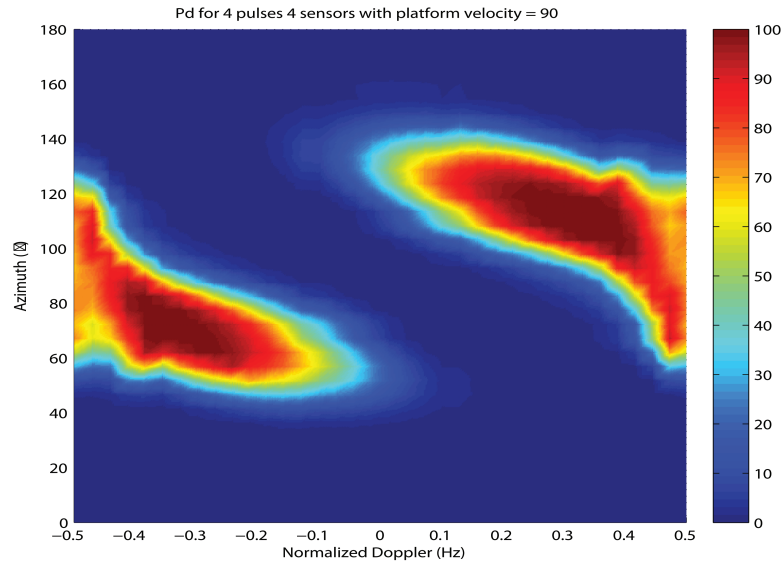
Figure 5.20: Coverage area analysis output, P_d for 4 pulses and 4 sensors.
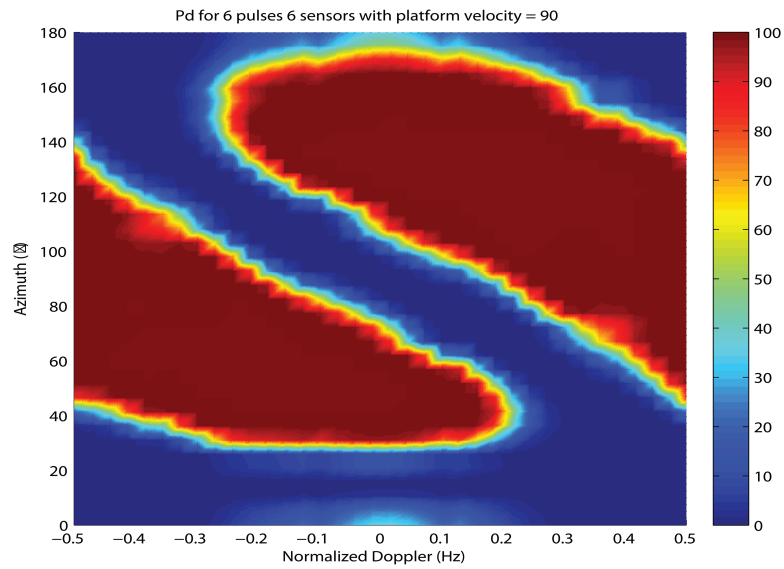
Figure 5.21: Coverage area analysis output, P_d for 6 pulses and 6 sensors.

CHAPTER 6

CONCLUSION AND FUTURE WORK

6.1 Conclusions

In this thesis, interference cancelation using space-time adaptive processing and using space-time adaptive processing in coverage area analysis are investigated. A model was developed for a generic radar system. Basic requirements for coverage analysis and why radar designers needs such a tool are presented. Fully adaptive space-time adaptive processors that simultaneously combines the received signals from antenna array elements during one CPI were introduced.

It is successfully shown that space-time adaptive processing can be used to suppress wideband jammer effectiveness together with ground clutter effects. The main idea behind the interference cancelation for airborne or spaceborne radar is to design a multidimensional filter to suppress incoming jammer signals and clutter echoes. It has been shown that the target would be detected under hostile electronic countermeasures using space-time adaptive processing, while traditional radars can not distinguish target. Performance of space-time adaptive processing is tested for different radar parameters.

The target detection performance of STAP is tested via coverage area analysis along Doppler-azimuth domain. It is shown that under hostile electronic countermeasures, target detection is not possible by traditional radar signal processing tools while space-time adaptive processing achieves target detection.

Throughout this thesis study, it is assumed that the processor already has the statistics of the interference. However, in practical applications the processor needs to estimate the statistics

of the interference sources in order to calculate the adaptive weight vector. The real challenge in this topic is estimating the statistics of the interference sources in real time applications.

As a conclusion, this thesis has given an insight about modeling the received signal from both stationary and non-stationary scatterers for airborne or spaceborne radars. It has been shown that interference sources are suppressed effectively by using appropriate space-time adaptive processing filters. Consequently, we showed that coverage area of a traditional radar can be increased by replacing the traditional radar with a space-time adaptive processing radar.

6.2   Future Work

This study used the mathematical model for the statistics of the interference sources. Future work of this study should include estimating the statistics of the interference sources.

Constant clutter model is used to calculate the clutter echoes. Future work of this study should include the usage of height profile data in order to model clutter effects more realistically. Also, from propagational point of view this study should include more accurate propagation calculation techniques such as *parabolic wave equations* in order to calculate propagation factor more accurately.

Throughout this thesis, linear arrays are used for signal modeling. Future work of this study may include planar arrays for received signal modeling, in order to eliminate ambiguity in elevation.

REFERENCES

[1] John S. Hall et al. In John S. Hall, editor, *Radar Aids To Navigation*, Radiation Laboratory Series. McGraw - Hill Book Company, Inc., 1947.

[2] Merrill I. Skolnik. *Introduction To Modern Radar Systems*. McGraw - Hill Book Company, Inc., 1221 Avenue of the Americas, New York, NY, 10020, 2001.

[3] David K. Barton. *Modern Radar System Analysis*. Artech House, 685 Canton Street Norwood, MA 02062, 1 edition, 1988.

[4] Bassem R. Mahafza. *Radar Systems Analysis and Design Using MATLAB*. Chapman and Hall, 2000.

[5] Ramon Nitzberg. *Radar Signal Processing And Adaptive Systems*. Artech House, 1999.

[6] David K. Barton and Sergey A. Leonov. *Radar Technology Encyclopedia*. Artech House, 685 Canton Street Norwood, MA 02062, 1 edition, 1998.

[7] Lamont V. Blake. *Radar Range - Performance Analysis*. Artech House, 685 Canton Street Norwood, MA 02062, 1 edition, 1986.

[8] Nadav Levanon. *Radar Principles*. John Wiley and Sons, 1 edition, 1988.

[9] Mark A. Richards. *Fundamentals Of Radar Signal Processing*. McGraw - Hill Book Company, Inc., 1221 Avenue of the Americas, New York, NY, 10020, 2 edition, 2005.

[10] Joseph R. Guerci. *Space - Time Adaptive Processing for Radar*. Artech House, 685 Canton Street Norwood, MA 02062, 1 edition, 2003.

[11] Alan V. Oppenheim and Ronald W. Schafer. *Discrete - Time Signal Processing*. Prentice Hall, Upper Saddle River, New Jersey 07458, 1 edition, 1989.

[12] Temel E. Tuncer. *Sensor Array Signal Processing Lecture Notes*. Electrical and Electronics Engineering. Middle East Technical University, 2010.

[13] Richard Klemm. *Principles of Space Time Adaptive Processing*. The Institution of Engineering and Technology, London, UK, 3 edition, 2006.

[14] James Ward. Space time adaptive processing for airborne radar. Technical Report 1015, Lincoln Laboratory, Dec. 1994.

[15] William L. Melvin. Stap overwiev. *IEEE*, 19(1):19–35, 2004.

[16] Peyton Z. Peebles. *Probability, Random Variables, Random Signal Principles*. McGraw - Hill Book Company, Inc., 1221 Avenue of the Americas, New York, NY, 10020, 4 edition, 2000.

[17] Manson H. Hayes. *Statistical Digital Signal Processing and Modeling*. John Wiley and Sons, Inc., 1 edition, 1996.

[18] Richard Klemm. Introduction to space-time adaptive processing. *Electronics & Communication Engineering Journal*, pages 5–12, Feb. 1999.

[19] Charles W. Therrien. *Discete Random Signal And Statistical Signal Processing*. Signal Processing Series. Prentice-Hall, Upper Saddle River, New Jersey 07458, 1992.

[20] Areps coverage. http://www.public.navy.mil/spawar/Pacific/55480/Pages/SoftwarePrograms, last accessed on 24.08.2011.

[21] Carpet coverage. http://www.tno.nl/, last accessed on 24.08.2011.

[22] Multipath. http://zone.ni.com/devzone/cda/ph/p/id/61, last accessed on 24.08.2011.

[23] Attenuation by atmospheric gases. Rec ITU-R P.676-7, 2007.

[24] Reference standard atmospheres. Rec ITU-R P.835-4, 2005.

[25] Specific attenuation model for rain for use in prediction methods. Rec ITU-R P.838-3, 2005.

[26] J.E. Brennan, L.E. Mallet and I.S. Reed. *Adaptive arrays in airborne MTI radar*, volume AP-24. Sept. 1976.

[27] R. Klemm and Dr. Ing. *Adaptive clutter suppression for airborne phased array radars*, volume 130. Fab. 1983.

[28] Yeheskel Haimovich, Alexander M. Bar-Ness. An eigenanalysis interference canceler. *IEEE*, 39(1):76–84, 1991.

APPENDIX A

PARTIALLY ADAPTIVE SPACE-TIME ADAPTIVE PROCESSING

The fully adaptive techniques are impractical for the reasons of computational cost. Partially adaptive STAP algorithms will be considered in this section. The structure of a generic partially adaptive algorithm will be presented [14].

A.1   A Generic Architecture

Partially adaptive processor transforms a large set of input signals and transforms them into considerably small number of signals. Block diagram of this processor is given in Figure A.1.

The transformed data is $D \times 1$. The transformation is done by using $MN \times D$ preprocessor matrix

$$\tilde{\mathbf{x}} = \mathbf{T}\mathbf{x} \qquad \text{(A.1)}$$

where $\mathbf{x}$ is the received signal composed of target signal interference signal and noise signal, $\mathbf{x}\,(t)$ and is the preprocessor matrix of size $MN \times D$. The transformed data may be decomposed into two by using target signal and interference plus noise signal separately.

$$\tilde{\mathbf{x}} = \tilde{\mathbf{x}}_T + \tilde{\mathbf{x}}_i, \qquad \text{(A.2)}$$

where T defines target signal and i defines the interference plus noise signal. After data transformation $D \times D$ dimensionally reduced covariance matrix is computed as
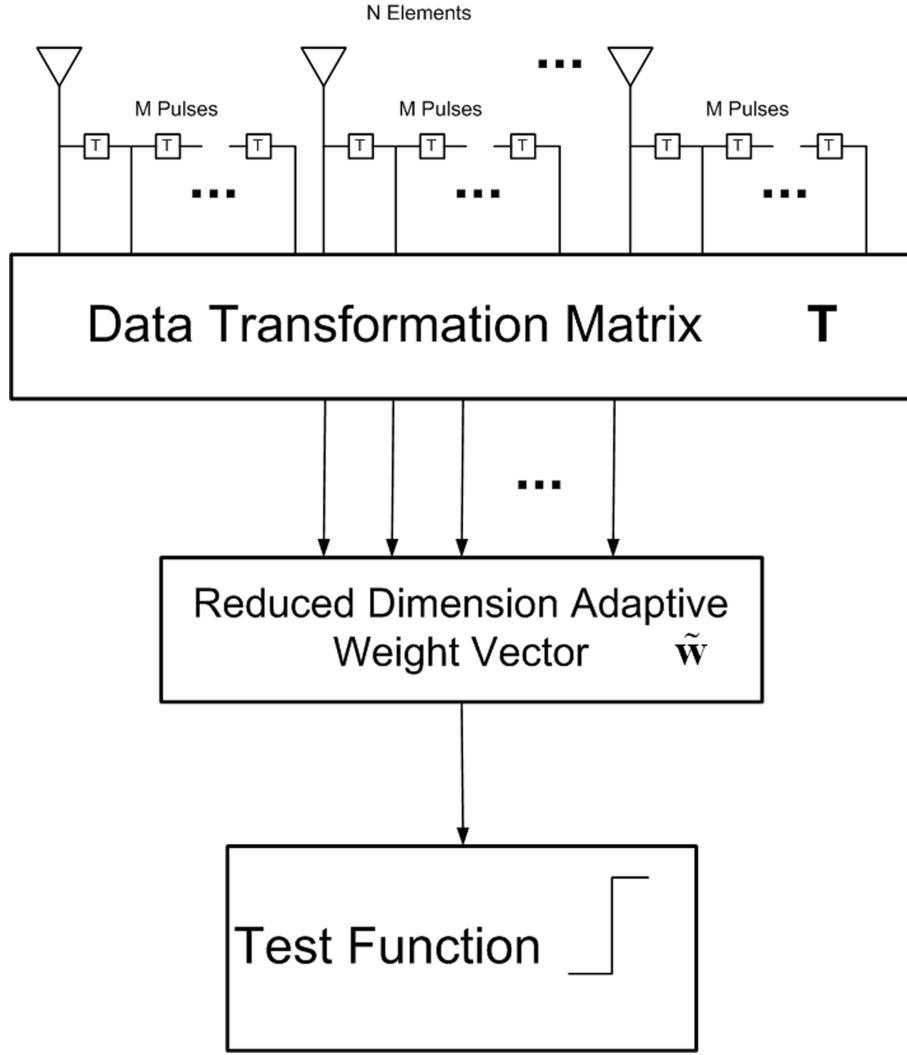
Figure A.1: Block diagram of a generic partially adaptive processor.

$$\tilde{\mathbf{Q}} = E\left\{\tilde{\mathbf{x}}\tilde{\mathbf{x}}^H\right\} = \mathbf{T}^H\mathbf{Q}\mathbf{T}, \tag{A.3}$$

where $\mathbf{Q}$ is the covariance matrix of original received interference plus noise signal. The reduced dimensional desired response is calculated by projecting the desired response for fully adaptive case to transformation space for partially adaptive processing. The formalization for the reduced dimensional desired response is given in eq. (A.4).

$$\tilde{\mathbf{s}} = \mathbf{T}^H\mathbf{s}, \tag{A.4}$$

where **s** is the desired response for the fully adaptive case.

The adaptive processor weight vector for partially adaptive processor is calculated by using reduced dimensional covariance matrix and reduced dimensional desired vector as

$$\tilde{\mathbf{w}} = \gamma \tilde{\mathbf{Q}}^{-1} \tilde{\mathbf{s}}. \tag{A.5}$$

The major issue of this processing technique is the design of **T**. It is desirable to design **T** with $D \ll MN$ as small as possible while achieving as close to fully adaptive (optimum) performance as possible.